

Application of in situ testing in tailing dams, emphasis on liquefaction: Case-history

A. Viana da Fonseca

University of Porto, Faculty of Engineering, Department of Civil Engineering, Portugal

ABSTRACT: Geotechnical design and the solutions for construction of tailings dams resulting from the mining industry operations, specially the evaluation of the possibility of flow liquefaction responsible for the collapse of several dams, has been mobilizing the attention of researchers and engineering practitioners. The investigation of water table position, aquifer boundaries, physical conditions and density of the deposited materials demand for site characterization and determination of short and long term properties of tailings materials, constitute crucial requirements for engineering with tailings. An increasing emphasis on in situ tests with emphasis to CPTU and DMT tests, and geophysical survey for seismic wave profiling, which allow for thorough study of segregation, state condition, shear strength and consolidation properties, identifying the essential features that link some of the deduced parameters, such as saturation level, drainage conditions, liquefaction potential—both triggering or post-behavior, has been addressed lately with increase frequency. In this paper some of these potentialities will be discussed in the light of recent published approaches and two case-histories are presented transcribing some papers that describe them.

1 INTRODUCTION

There are three basic types of tailings dams: downstream, upstream, and centerline (Vick 1983; Carrier 2003). Downstream construction is used when there is a sufficient volume of the coarse fraction of the tailings to construct the entire dam (Jamiolkowski et al. 2010). A downstream dam is raised in a series of lifts as the level of the tailings rises during the course of mining and processing. Upstream construction is used when the tailings are suitable for raising a dam. The coarse fraction of the tailings (i.e. sand) is separated from the fine fraction (i.e. silt and clay, usually called “slimes”) by means of either spigots or cyclones that are periodically moved along the crest of the embankment as it is raised. Slurry of fine material runs down the beach into the pond; the coarse material is used to construct the shell in a series of lifts. The centerline of the crest moves upstream as each new lift is added. Centerline construction is a hybrid of the downstream and upstream methods. Coarse shell material is added in lifts, both upstream and downstream, so that the centerline of the crest of the dam remains in the same location throughout the life of the structure. Figure 1 illustrates these processes.

Within the entire range of failure modes that have occurred at tailings impoundments static liquefaction is likely the most common, and at the same time likely the least understood (Blight 2009).

Although the upstream construction is the most popular type of embankment for tailings dams, since it is a low cost process, it is a high risk operation, particularly because (a) upstream dams are particularly susceptible to liquefaction under seismic ground motion and (b) dam stability is endangered if the raising rate of the dam is high due to excess pore pressure built within the deposit during construction (Schnaid et al. 2007). Tailings have specific properties, different of naturally deposited materials, so they have to be tested in field and laboratory to be calibrated and their mechanical characteristics can be assessed by the most effective techniques.

Tailing dams may be critical, especially where there is improper handling and management. Examples of that are the disasters at tailings facilities of Aznalcóllar (Spain), in 1998, and Baia Mare (Romania), in 2000, with major threats to the environment and human life. This risk is high in the upstream method, since it provides only a thin shell with instability implications. Unlike the large dams of water reservoirs, tailings dams are constructed without any impervious core.

Process and rainfall water seeps through the dam towards its free face. Uncontrolled water flow through, beneath or—in the worst case—over the dam can lead to a critical loss of stability. In handling large amounts of inhomogeneous wet slurries, water management is a key safety factor. Deficient water management is one of the main causes of

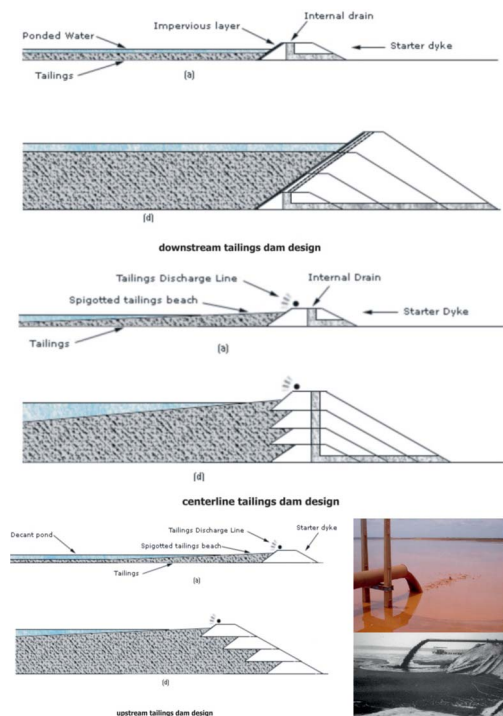


Figure 1. Three types of construction systems in tailings dams: downstream, upstream, and centreline (<http://www.ecm-ing.com/tailings%20eng/>).

accidents and hazards emanating from tailings facilities (Davies et al. 2002). These authors resume the risk as follows: “static liquefaction, and the resulting flowslide of liquefied tailings materials, is shown to be a relatively common phenomenon among the more dramatic tailings impoundment failure case histories. Static liquefaction can be a result of slope instability issues alone, or can be triggered as a result of other mechanisms”. Continuing citing Davies et al. (2002), it is known that “loose sands could behave in a puzzling manner, and has been recognized as early as the first use of the term “liquefies” in our context by Hazen (1920) reporting on the failure of the Calaveras Dam during construction. Writing in German, Terzaghi (1925) defined the essential processes of liquefaction and the subsequent lecture by Casagrande (1936) formed the basis for practice at that time. In this early paper, and refined in subsequent work (Casagrande 1976), the critical void ratio concept was clearly defined. This method used drained direct shear or triaxial tests to define the void ratio at which neither drained contraction or dilation occurs at high strain, and observed that there was a unique relation between this so-defined critical void ratio and the log of effective stress. But, in

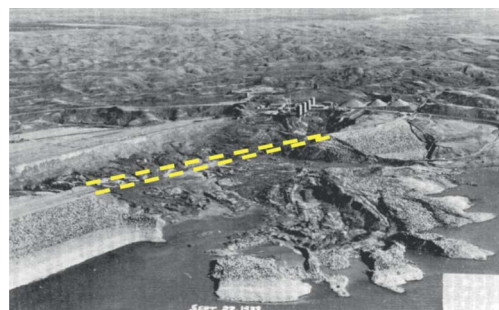


Figure 2. Oblique view of Fort Peck Dam failure—1938 (Davies et al. 2002).

1938, the hydraulic fill Fort Peck Dam failed during construction (Middlebrooks 1940). As noted by Morgenstern and Küpper (1988) the collapse of the Fort Peck Dam (Figure 2) constituted a watershed in the evolution of hydraulic fill methods for dam construction in North America and marked an abrupt decline in the technique [but not for tailings dam construction].

2 IN SITU TESTS FOR RISK ANALYSIS IN TAILING DAMS

2.1 Seismic Dilatometer (SDMT) in tailing dams

Recent research projects have been pursuing in situ tests (with emphasis for piezocone) and laboratory tests (triaxial) to be carried out in active iron ore, gold and alumina residue storages (e.g., Schnaid 2005; Schnaid et al. 2004, 2008).

The liquefaction analysis of sloping ground in these difficult geotechnical conditions (i.e., tailings subject to a static driving shear stress) is a challenge. The estimation of the residual or liquefied shear strength of these soils, require special procedures in laboratory testing over field samples obtained by difficult sampling techniques, such as ground freezing methods (Robertson et al. 2000) or samples obtained by high-quality tube samples coupled with procedures for “correcting” the shear strength for disturbance during sampling and testing (Castro 1975).

Cone penetration test (CPT-based) relationships allow to evaluate the susceptibility to strength loss and liquefied shear strength for a wide range of soils (Olson & Stark 2003; Robertson 2010). In fact, some tests have been pointed out as particularly more efficient and cost effective as a direct-push method using multi-measurement in-situ devices, such as the seismic cone penetration test with pore pressure measurements (SCPTu) and the seismic flat dilatometer test (SDMT). Since the CPTu is about 3 to 4 times faster, collects more frequent data and

is less expensive than the DMT, the CPTu is increasingly the preferred primary in-situ test. The continuous nature of the CPTu results provide valuable information about soil variability that is difficult to match with sampling and laboratory testing.

There are a large number of potential geotechnical parameters and properties necessary for the analyses of safety in these projects, but some have major importance: in-situ state, strength, stiffness, compressibility and conductivity. In-situ state represents quantification of the density and compactness of the soil, as well as factors such as cementation. For most soils, in-situ state is captured in terms of either relative density (D_r) or state parameter (ψ) for coarse-grained soils and over-consolidation ratio (OCR) for fine-grained soils. These 'state' parameters essentially identify if soils will be either dilative or contractive in shear (Robertson 2012). CPT has been pointed as very sensitive to the determination of soil stratigraphy and the identification of soil type. This has been accomplished using charts that link cone parameters to soil type. Robertson (2010b) suggested an update on the soil behavior type (SBT) charts, as shown in Figure 3. The updated charts, that are dimensionless and color coded for improved presentation, define 9 consistent SBT zones.

As described in this conference (Robertson 2012), Jefferies & Davies (1993) identified that a soil behavior type index, $I_{c,JD}$, could represent the SBTn zones in the Q_t-F_r chart where, $I_{c,JD}$ is essentially the radius of concentric circles that define the boundaries of soil type. Robertson and Wride, (1998) modified the definition of I_c to apply to the Robertson (1990) Q_t-F_r chart, as defined by:

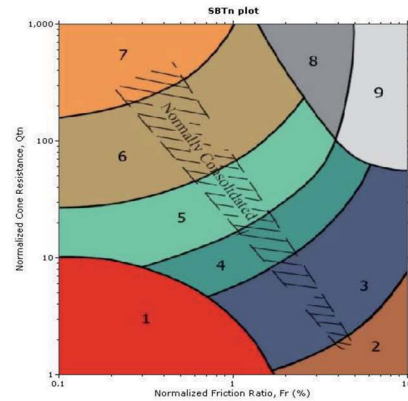
$$I_c = [(3.47 - \log Q_t)^2 + (\log F_r + 1.22)^2]^{0.5}$$

Knowing that the state parameter (ψ) is defined as the difference between the current void ratio, e , and the void ratio at critical state, e_{cs} , at the same mean effective stress for coarse-grained (sandy) soils, Jefferies & Been (2006), based on critical state concepts, provided a detailed description of the evaluation of soil state using the CPT. They describe in detail that the problem of evaluating state from CPT response is complex and depends on several soil parameters, being this resumed in this conference (Robertson 2012). Robertson (2009a) developed contours of state parameter (ψ) on the updated SBTn Q_m-F chart for uncemented Holocene age soils. The contours, that are shown on Figure 4, are approximate since stress state and plastic hardening will also influence the estimate of in-situ soil state in the coarse-grained region of the chart (i.e. when $I_c < 2.60$) and soil sensitivity for fine-grained soils.

An area of uncertainty in the approach used by Jefferies and Been (2006) is the use of Q_{t1} rather

SBT zone	Proposed SBT description
1	Sensitive fine-grained
2	Clay - organic soil
3	Clays: clay to silty clay
4	Silt mixtures: clayey silt & silty clay
5	Sand mixtures: silty sand to sandy silt
6	Sands: clean sands to silty sands
7	Dense sand to gravelly sand
8	Stiff sand to clayey sand*
9	Stiff fine-grained*

* Overconsolidated or cemented



where;

$$Q_{t1} = (q_t - \sigma_{vo})/\sigma_{vo}$$

$$F_r = [(f_s/(q_t - \sigma_{vo}))] 100\%$$

$$B_q = (u_2 - u_0)/(q_t - \sigma_{vo}) = \Delta u/(q_t - \sigma_{vo})$$

and:

$$\sigma_{vo} = \text{in-situ total vertical stress}$$

$$\sigma'_{vo} = \text{in-situ effective vertical stress}$$

$$u_0 = \text{in-situ equilibrium water pressure}$$

$$\Delta u = \text{excess penetration pore pressure} = (u_2 - u_0)$$

Figure 3. Updated Soil Behaviour Type (SBT) charts based on either normalized CPT (Robertson 2010b).

than Q_{m1} . Figure 4 uses Q_m since it is believed that this form of normalized parameter has wider application, although this issue may not be fully resolved for some time. The contours of ψ shown in Figure 4 were developed primarily on laboratory test results and validated with well documented sites where undisturbed frozen samples were obtained (Wride et al. 2000). Jefferies and Been (2006) suggested that soils with a state parameter less than -0.05 (i.e. $\psi < -0.05$) are dilative at large strains.

Robertson and Wride (1998), based on a large database of liquefaction case histories, suggested a CPT-based correction factor to correct normalized cone resistance in silty sands to an equivalent clean sand value ($Q_{m,cs}$) using the following:

$$Q_{m,cs} = K_c Q_m$$

Where K_c is a correction factor that is a function of grain characteristics (combined influence

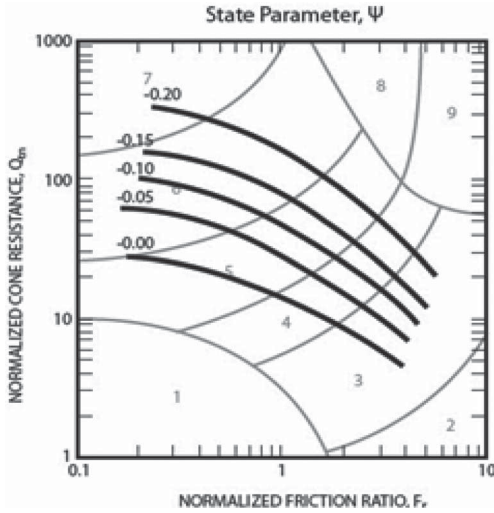


Figure 4. Contours of estimated state parameter, ψ (thick lines), on normalized SBTn Q_m-F_c chart for uncemented Holocene-age sandy soils (After Robertson 2009).

of fines content, mineralogy and plasticity) of the soil that can be estimated using I_c as follows:

if $I_c \leq 1.64$: $K_c = 1.0$

if $I_c > 1.64$:

$$K_c = 5.581I_c^3 - 0.403I_c^4 - 21.63I_c^2 + 33.75I_c - 17.88$$

Robertson (2010c) suggested a simplified and approximate relationship between ψ and $Q_{m,cs}$, as follows:

$$\psi = 0.56 - 0.33 \log Q_{m,cs}$$

2.2 Seismic dilatometer (SDMT) in tailing dams

The seismic dilatometer (SDMT) is a combination of the standard flat dilatometer (DMT) equipment (Marchetti 1980; Marchetti et al. 2001) with a seismic module for the down-hole measurement of the shear wave velocity V_S . First introduced by Hep-ton (1988), the SDMT was subsequently improved at Georgia Tech, Atlanta, USA (Martin & Mayne 1997, 1998; Mayne et al. 1999) and is now in its maturity, being accepted as a very consistent and effective tool for evaluation of liquefaction potential, taking into account ageing and (or) stress history of soils, as reported by Monaco & Marchetti (2007).

A new SDMT system incorporating two waves' receivers, therefore with a clear ("true") length which gives rise to a more reliable velocity (Figure 4) has been recently developed in Italy. The seismic module (Figure 4a) is a cylindrical element placed above the DMT blade, equipped with two receivers located at 0.5 m distance. The signal

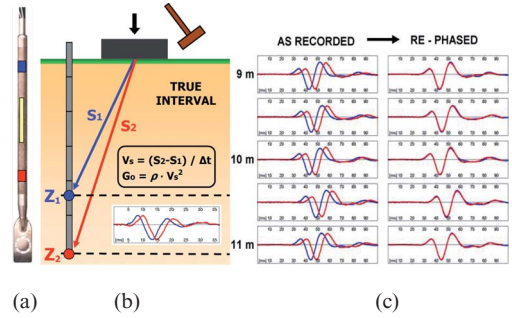


Figure 5. (a) DMT blade and seismic module. (b) Schematic layout of SDMT. (c) Example of seismograms obtained by SDMT at various test depths (Monaco & Marchetti 2007).

is amplified and digitized at depth (Monaco & Marchetti 2007). The shear wave source at the surface (Figure 1b) is a pendulum hammer which hits horizontally a steel rectangular base pressed vertically against the soil and oriented with its long axis parallel to the axis of the receivers, so that they can offer the highest sensitivity to the generated shear wave. This configuration avoids possible inaccuracy in the determination of the "zero time" at the hammer impact and the coupling of seismograms recorded by the two receivers at a given test depth (Figure 4b) corresponds to the same hammer blow and not to different blows in sequence, not necessarily identical, improving the repeatability of V_S measurements. With V_S measurements obtained every 0.5 m of depth, the determination of the delay from the seismograms obtained by SDMT is generally well-conditioned (Figure 5c).

The possibility of using V_S as an index of liquefaction resistance is widely recognized, being the most popular CRR- V_S correlation (Figure 6) the one proposed by Andrus and Stokoe (2000). CRR is obtained as a function of an overburden-stress corrected shear wave velocity $V_{S1} = V_S(p_a/\sigma'_{v0})^{0.25}$, where V_S = measured shear wave velocity, p_a = atmospheric pressure (100 kPa), σ'_{v0} = initial effective vertical stress (same units as p_a). Andrus et al. (2004) introduced age correction factors to extend the original correlation by Andrus and Stokoe (2000) to soils older than Holocene. Their CRR- V_{S1} relationship (curves in Figure 6) is approximated by the equation:

$$CRR = \left[0.022 \left(\frac{K_{a1} V_{S1}}{100} \right)^2 + 2.8 \left(\frac{1}{V^*_{S1} - K_{a1} V_{S1}} - \frac{1}{V^*_{S1}} \right) \right] K_{a2}$$

where V^*_{S1} = limiting upper value of V_{S1} for liquefaction occurrence ($V^*_{S1} = 200$ m/s for the curve for fines content $\geq 35\%$, $V^*_{S1} = 215$ m/s for the curve for fines content $\leq 5\%$, V^*_{S1} varies linearly from 200 to 215 m/s for fines content between 35 and 5%),

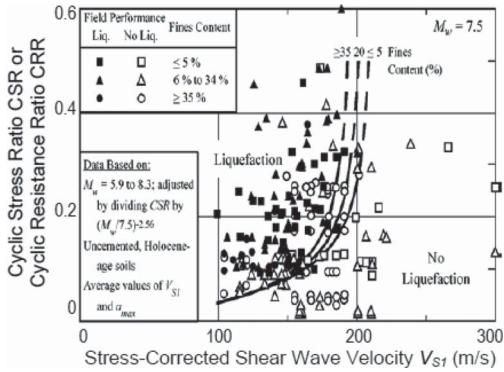


Figure 6. Curves for evaluating CRR from shear wave velocity V_s for clean, uncemented soils with liquefaction data from compiled case histories (Andrus and Stokoe 2000).

K_{a1} = factor to correct for high V_{S1} values caused by aging, K_{a2} = factor to correct for influence of age on CRR. As stressed by Monaco & Marchetti (2007), magnitude scaling factors should be used to scale—see equation (for magnitude $M_w = 7.5$ earthquakes) to different magnitudes. Both K_{a1} and K_{a2} are 1 for uncemented soils of Holocene age. For older soils, suggested K_{a1} values (mostly in the range 0.6 to 0.8) are derived from SPT- V_{S1} relationships (e.g. Ohta and Goto 1978, Rollins et al. 1998, or site specific). Lower-bound values of K_{a2} (1.1 to 1.5) are based on the study by Arango et al. (2000). Andrus et al. (2004) remarked, however, the high associated uncertainty and the need of additional work to quantify the influence of age on CRR, as well as on V_s .

Before the possibility of using seismic waves' capabilities in SDMT, the original dilatometer (DMT) has been explored for CRR evaluation. Marchetti (1982), Robertson and Campanella (1986), Reyna and Chameau (1991), suggested that the horizontal stress index K_D from DMT ($K_D = (p_0 - u_0)/\sigma'_{v0}$) is a suitable index parameter of liquefaction resistance. Comparative studies have indicated that K_D is highly sensitive to factors that increase liquefaction resistance like stress history, ageing, cementation, structure (to which CPT is not by itself so sensitive (Huang and Ma (1994), except if combined with V_s measurements. G_0/q_c is influenced by relative density and effective stress as well as age and cementation (e.g. Eslaamizaad & Robertson 1996; Fahey et al. 2003; Schnaid et al. 2004), but should not be used by itself to reduce uncertainty in liquefaction-triggering correlations. The empirical parameter K_G , as defined in the following equation (after Rix & Stokoe 1992), can be used to account for sand relative density and effective

stress level on the correlation between G_0 and q_c (Schneider & Moss 2011):

$$K_G = \frac{G_0/q_c}{\left[(q_c/p_{ref}) / (\sigma'_{v0}/p_{ref})^{0.5} \right]^m} = \frac{G_0/q_c}{q_{c1N}^{-m}}$$

where σ'_{v0} is the initial in situ vertical effective stress, p_{ref} is a reference stress equal to 100 kPa, m is an empirical exponent typically taken as 0.75 (Rix & Stokoe 1991; Schneider et al. 2004) and q_{c1N} is the stress normalized cone tip resistance using a median sand overburden stress exponent of 0.5 (Moss et al. 2007). As noted by Robertson & Campanella (1986), it is not possible to separate the individual contribution of each factor on K_D . On the other hand, a low K_D indicates that none of the above factors is high, i.e. the sand is loose, uncemented, in a low K_0 environment and has little stress history. A sand under these conditions may liquefy or develop large strains under cyclic loading. The most significant findings supporting a well-based CRR- K_D correlation are the sensitivity of DMT in monitoring soil densification (Schmertmann et al. 1986 and Jendebj 1992) and to prestraining (Jamiolkowski and Lo Presti 1998), and, specifically the sensitivity of K_D to ageing (Monaco & Schmertmann 2007).

Yu (2004) proved that K_D is an index that reflects the in situ state parameter ψ (ξ_0 in that work) and presented a correlation between K_D and ξ_0 in sands (Figure 7) which strongly encourage efforts to develop methods to assess liquefiability by DMT.

Figure 8 shows that data-points obtained at sites where liquefaction had occurred (mostly in

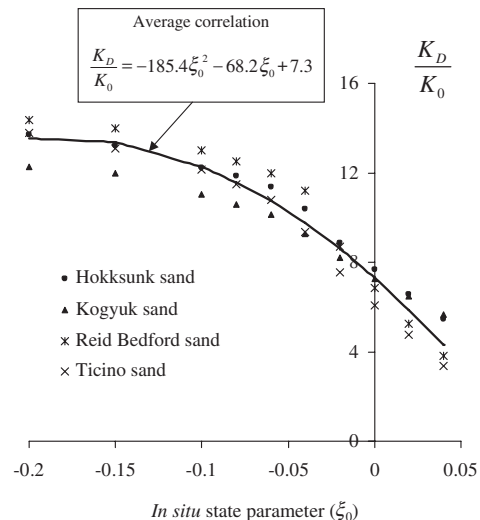


Figure 7. Average correlation for deriving in situ state parameter, $\xi_0 (= \psi)$ as suggested by Yu (2004).

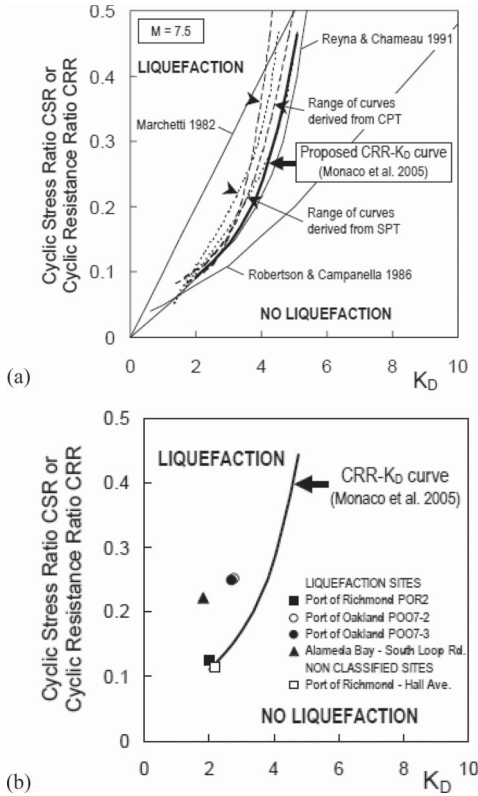


Figure 8. (a) CRR- K_D curves for evaluating liquefaction resistance from DMT (Monaco et al. 2005). (b) Comparison of CRR- K_D curve by Monaco et al. (2005) and Loma Prieta 1989 earthquake liquefaction datapoints (after Mitchell et al. 1994).

hydraulic sandfills) are correctly located in the “liquefaction” side. Grasso and Maugeri (2006) further updated the CRR model by Monaco et al. (2005) into:

$$CRR_{7.5} = 0.0908K_D^3 - 1.0174K_D^2 + 3.8466K_D - 4.5369$$

$$CRR_{7.5} = 0.0308e^{0.605K_D}$$

$$CRR_{7.5} = 0.0111K_D^{2.5307}$$

Tai et al. (2009) examined these CRR- K_D curves, the SPT and CPT-based liquefaction case histories presented by Idriss & Boulanger (2006) and Robertson & Wride (1998), respectively, transformed SPT- and CPT based in CRR- K_D curves along with the transformed data points of the SPT- and CPT-based liquefaction case histories, getting into a new proposal for the DMT-based CRR- K_D :

$$CRR_{7.5} = \exp \left[\left(\frac{K_D}{8.8} \right)^3 - \left(\frac{K_D}{6.5} \right)^2 + \left(\frac{K_D}{2.5} \right) - 3.1 \right]$$

A long discussion has been developed around the arguments on the better applicability of CPT (we will ignore SPT-based data for its insensitivity to characterize soft or loose geomaterials) or DMT for liquefaction evaluation. This turns to a question that should be faced in terms of complementary approaches and not as concurrent. Marchetti (2010) compiled extensive data presented by several authors, including an extensive Calibration Chamber comparative program at Korea University, showing that K_D is considerably more sensitive than q_t to Stress History (including aging). Schnaid (2009) point out that q_t is not very sensitive to Stress History. Being this factor important for liquefaction, increasing substantially CRR, being difficult for CPT to have, by itself, high reliability to assess sand liquefiability, requiring a new in situ device, more sensitive to effects of past *stress-strain histories* and some evidences point to the higher sensitivity of K_D to Stress History suggesting that this DMT parameter has a good link with CRR.

2.3 Limiting values of V_{s1} and K_D for liquefaction occurrence

There are some fruitful discussions (Roberston 2009; Marchetti 2010; Marchetti 2011) on which parameter is more sensible to resistance to liquefaction, due to the important effects of stress history and aging: K_D —a direct parameter of DMT test interpretation—, or q_t (or its normalized values Q_{t1}), or V_s (or its normalized values V_{s1}) determined in geophysical testing, which now includes the seismic waves’ capabilities (Monaco & Marchetti 2007). One of the key points of this discussion, as already been referred, above is the eventual higher sensitivity of K_D to aging, and this is not strange to the fact that this a parameter that has correspondence to normalized key parameters of CPT and Q_{t1} , as proved by Robertson (2009), although somewhat influenced by the normalization technique. This author proposes correlations between the values of the soil-type (I_c , from CPT, and I_D , from DMT) and mechanical behavior indices (Q_{t1} , from CPT, and K_D , from DMT), expressed in the contours of Figure 9.

This may be, however, still in arguing since Marchetti (2011) defends that (sic) the big difference between CPT and DMT is that DMT provides the parameter K_D related to the stress history (a fundamental piece of information and a protagonist in the DMT interpretation), whereas q_c is unaccompanied by a similar parameter containing information about stress history.

In the light of this discussion the author states that’s the engineering application for which translation formulas (current or future) for

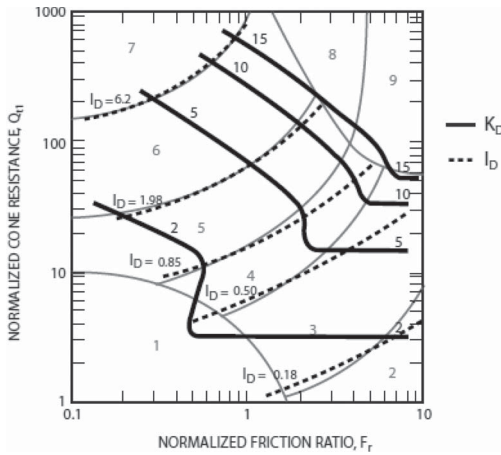


Figure 9. Proposed contours of DMT K_D and I_D on the CPT normalized SBT Q_n-F_r chart (Robertson 2009).

estimating K_D from CPT data are believed to be too inaccurate (sic), is the estimation of the sand liquefaction resistance [cyclic resistance ratio (CRR)] on the basis of K_D . Reporting to the paper by Marchetti (2010), where a compilation of data showing that K_D is considerably (“sic”) more sensitive than q_t (or Q_{t1}) to stress history and aging, the author defends that no translation formula could reconstruct K_D values incorporating such sensitivity if the reconstruction is on the basis of q_t , which is “almost independent of past straining along the K_D -line” (Baldi et al. 1985) and “is not very sensitive to stress history” (Schnaid 2009), so important for liquefaction evaluation.

Comparisons based on parallel measurements of K_D and V_s obtained by SDMT at several sandy sites have shown that V_s (V_{s1}) and K_D would provide, in general, substantially different estimates of CRR, leaving open the question “which CRR should be given greater weight” when parallel analyses by K_D and V_s produce contradictory predictions (Monaco et al. 2005; Monaco & Marchetti 2007; Monaco & Schmertmann 2007; Marchetti et al. 2008).

Another difference in the correlations CRR- V_s and CRR- K_D may be noted in the limiting values of V_{s1} and K_D for which liquefaction occurrence can be definitely excluded. The measured V_{s1} values, normalized with respect to the vertical effective stress, generally result in values greater than the value of 160 m/s which is regarded by Robertson et al. (1992) as the upper bound shear velocity above which the tailings dilate in shear.

2.4 Geophysical tests for risk analysis in tailing dams

Non-destructive geophysical investigation methods of parameter evaluation and measurement are also being developed for the detection, assessment and improvement of the safety state of tailings dams and ponds. Geoelectrical (SIP), seismic and radar methods will be used to get information on the tailings dam structure and water content.

Most of the tailing dams are not structured, with transition zones between the tailings and the dam. Height and thickness of the several parts of the dam vary in the horizontal and vertical direction, being necessary to develop probabilistic methods for geotechnical stability analysis. As it is not possible to take more than just a few samples, the highly inhomogeneous structure of the tailings dams cannot be estimated with these methods only. Spectral Induced Polarization (SIP) and other geoelectrical methods have been reported to be valuable tools for investigating tailing dumps (Campbell & Fitterman 2000). In these cases the method was used to give a raw overview of the structure or the content of the dumps. GPR is another method for near surface investigations that may be used to this purpose. A short electromagnetic pulse is sent in the earth by an antenna, the reflected signals are received by another one. This is to be scribed used for evaluating the near surface structure of the dams and determine the position of the depth of the groundwater level. Finally, seismic methods should be considered, at least in specific points, as they rely on the generation, propagation and detection of mechanical waves. Common sources are hammers, weight drops and others. The interpretation of the arrival times of reflected and refracted waves from subsurface strata will give additional information on structure and water table.

3 ASSESSMENT OF TAILINGS DAMS LIQUEFACTION USING CRITICAL STATE SOIL MECHANICS CONCEPTS

3.1 How the binary void ratio-stress state may be key factor for liquefaction risk assessment

State parameter approaches have been applied with some success to the analysis of soil liquefaction both under cyclic and static loads, although the precise relationship between the two is perhaps less well understood (Viana da Fonseca et al. 2011). Compressibility is a key factor for the development of instability in both cases. This will be in direct accordance with the relative position of the state and the CSL so that the behaviour associated with the susceptibility to liquefaction can be

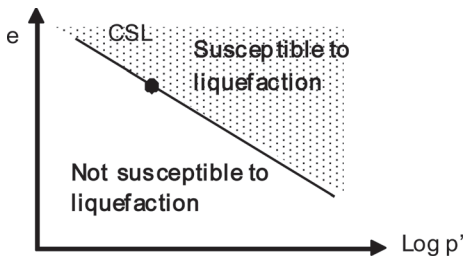


Figure 10. Criterion for flow liquefaction susceptibility based on state parameter concept (based on Kramer, 1996; Been & Jefferies 1985; and others).

analysed within a Critical State framework, providing a simple explanation for the patterns of behaviour typical of static liquefaction. Different classes of behaviour related to the current void ratio and stress state of the soil have been identified. Soils that have their in-situ states above the Critical State Line (Steady State Line) in the $e:\ln p'$ plane, with positive state parameters (Wroth & Bassett 1965; Been & Jefferies 1985) are more susceptible to liquefaction as illustrated in Figure 10. However, as highlighted by Carrera et al. (2011), Critical State Lines for sands are only linear in the $e:\ln(p')$ plane at high stress levels, and are typically curved lines that tend to a horizontal asymptote as p' reduces (e.g. Verdugo & Ishihara, 1996), often modelled as bilinear (e.g. Been et al. 1991). There are then some doubts about how state parameter should be applied to a curved CSL and whether the current location of the soil state relative to the curved line is important, i.e. whether the state parameter is measured from the straight CSL at high pressures or the flatter part at low pressures (Carrera et al. 2011).

There is also some ambiguity about the definition of liquefaction, although fundamentally it should be defined when the soil has genuinely reached a liquefied state, with zero effective stress and strength (Yamamuro et al. 2001). Within a Critical State framework it may seem that the phenomenon of static liquefaction is easily explained, as shown in the two examples of Figures 11 and 13. The data in Figure 11, by Carrera et al. (2011), are from a detailed investigation of the static liquefaction of Stava dam tailings (Figure 12). They tested a range of initial gradings and the data shown are for reconstituted samples of the clean poorly graded sand extracted from the tailings recovered from the Stava tailings dam disaster (Chandler & Tosatti 1995).

Figure 13 shows similar behaviour in an exhaustive study of the liquefaction risk of cycloning products from the disposal of gold tailings from Brazil, separated between coarser (underflow) and finer (overflow) fractions. Data for the overflow fraction are shown here, taken from an extensive programme of monotonic triaxial tests again on

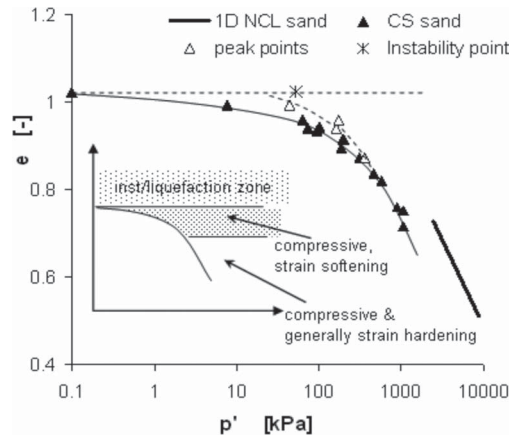


Figure 11. Variation of liquefaction behaviour with initial state for clean sand from Stava tailings (Carrera et al. 2011).

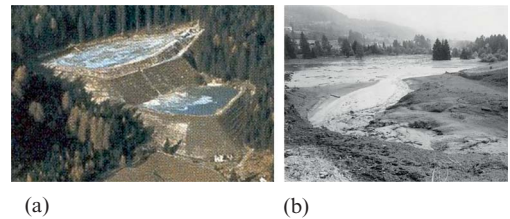


Figure 12. Stava tailings dam, before (a) and after the collapse (b) (<http://www.tailings.info/stava.htm>).

reconstituted samples (Bedin et al. 2011; Schnaid et al. 2012).

It is often assumed that the change in gradient of the Critical State Line in the $e:\ln p'$ plane at higher pressures is associated with particle breakage, as observed for example by Coop & Lee (1993), but this is not universally true and for the Stava tailings no breakage could be detected. In both cases the Critical State Line curves towards a horizontal asymptote at lower stress levels. Any sample with an initial state above that asymptote must therefore undergo instability and true liquefaction under undrained conditions, no matter what its initial stress level, as its stress path reaches $p' = 0$. At lower initial void ratios, where undrained loading brings the sample state towards the curved part of the Critical State Line, the soil will undergo a very large reduction in p' when loaded undrained, and give peak strength with dramatic strain softening.

This type of behaviour is often rather unhelpfully also referred to as liquefaction in the literature, but since the soil reaches a stable Critical

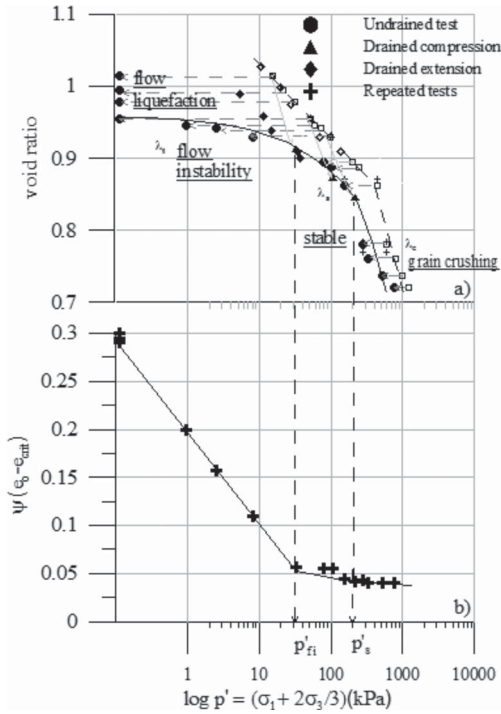


Figure 13. Critical State Soil mechanics applied to flow liquefaction, with curved Critical State Line (Bedin et al. 2011).

State, albeit at a low p' and hence strength, this is misleading. After all, there are plenty of soils that strain soften, but we do not say that they are liquefying. At high stress levels, where the Critical State and Normal Compression Lines tend to be parallel, the undrained stress-strain behaviour will be strain hardening or sometimes mildly strain-softening, and there can be no liquefaction of any kind. While other authors have seen slightly different patterns of behaviour for different soils (e.g. Yamamuro & Lade 1998), the general approach of distinguishing classes of behaviour by the state in the v (or e): $\ln p'$ plane remains successful, as far as, in principle, the state parameter should be applied to the specific curved CSL and not to the straight CSL at high pressures or the flatter part at low pressures. Figure 14 associates the same data of Figure 13 with measured values of shear wave velocities. A stable zone is observed at intermediate stresses with parallel NCL and CSL lines, while at high stresses, particle breakage under monotonic loading become dominant, changing the curvature of both lines. At the low stress range the onset of flow instability significantly changed the slope of the CSL relative to NCL reflecting the tendency for static liquefaction in undrained shear. Changes

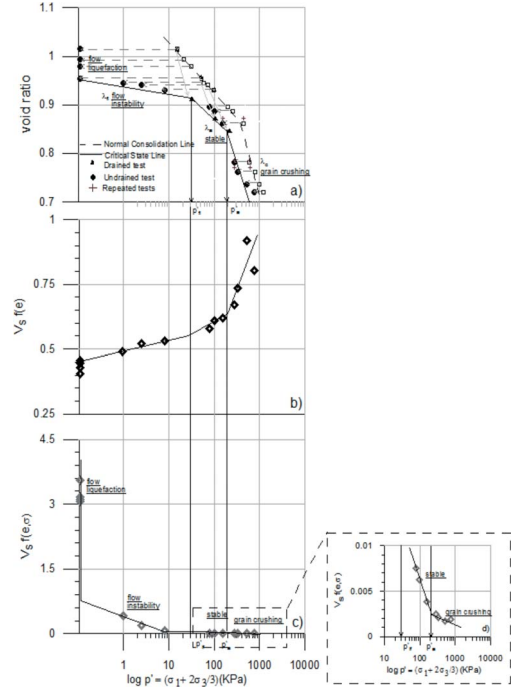


Figure 14. State parameter and state pressure index variation during testing (Bedin et al. 2011).

in slope of the CSL represent a transition of behaviour that is also captured in shear wave velocities variation.

Bedin (2010) present the extensive data recoiled along axial strain during undrained triaxial tests of the shear wave values, V_s , measured using bender elements (Viana da Fonseca et al. 2009), used to demonstrate that for any given test the initial shear velocity (V_{s0}), that is on consolidation state, values are greater than the V_s values measured at larger strain levels, reaching a minimum value at the very large strains at critical state.

These variations of shear wave velocity to mean stress, void ratio and state parameter are presented in Figure 14, with the purpose of representing measured V_s values in the framework of critical state.

In addition, Bedin (2010) presented a normalization of these values as a velocity ratio $V_{s,crit}/V_{s0}$ that is shown to range typically between 0.5 and 0.7 for the stable structure range, increasing up to 0.9 in the event of grain crushing and reducing to 0.3 to 0.5 when flow instability takes place.

Shear wave velocity (and therefore soil stiffness) depends upon interactions of state (void ratio, bonding, fabric, stress level) as well as strain level, stress history and stress path (e.g. Hardin 1978; Lo Presti 1995; Tatsuoka et al. 1997).

To account for these effects, the values of V_s have been expressed as a function of void ratio, $V_s f(e)$, as well as the void ratio and effective stress, $V_s f(e, p')$:

$$V_s f(e) = \frac{(V_s / V_{so})}{F(e)}$$

$$V_s f(e, \sigma) = \frac{(V_s / V_{so})}{(\sigma'_v)^{0.5} \cdot (\sigma'_h)^{0.5} \cdot F(e)}$$

These expressions are similar to those derived for the small strain shear modulus having the void ratio function $F(e)$ defined as $(2.17 - e)^2 / (1 + e)$, (Hardin & Richart 1963; Iwasaki et al. 1978). The normalized values of V_s are plotted in Figure 14. Both $V_s f(e)$ and $V_s f(e, p')$ are valuable means of characterising the transitional responses of the soil. For example, $V_s f(e, p')$ is of the order of 0.01 for a stable structure, increasing to up to 3 for liquefaction (300 times).

Based on these evidences, it is suggested that the response of the gold tailings can be expressed within the framework of critical state soil mechanics by assuming the behaviour illustrated in Figure 14.

The CSL is approximated by a three-linear model segment in the e - $\log(p')$ associated to different pressure levels leading to four distinct state conditions:

- Flow liquefaction: at low confining stresses this tailing exhibit a pronounced contractive response generating high excess pore pressures that ultimate leads to flow liquefaction instability coupled to a complete loss in shear strength and the development of excessive strains.
- Flow instability: ranging from low to moderate stress range, flow instability is associated to large deformations and high pore pressures that reduce the deviatoric stress at critical state relative to the deviatoric stress at the initial peak (without necessarily leading to liquefaction). For the tested tailing the pressure indicating the onset of flow liquefaction p'_{f1} was somewhere around 30 kPa. For stresses lower than p'_{f1} , a sample at its initial state (p'_o, e_o) located above the CSL experience larger reductions of its undrained shear resistance inducing a slope λ_f (flow) flatter than λ (stable). This implies that flow instability reduces with increasing confining pressures.
- Stable conditions: drained and undrained critical states coincide, defining a condition where the slope of the critical state line λ (stable) being essentially parallel to the slope of the normally consolidated line. This idealized behaviour is compatible to that conceived in most constitutive models of flow

liquefaction based on critical state soil mechanics (e.g. Dubujet & Doanh 2007; Doanh et al. 1997; Yamamuro and Lade 1997; Borja 2006; Andrade 2009).

- Particle breakage: for stresses greater than the stress corresponding to shear induced grain crushing p'_c the soil is able to reach denser states at critical state and as a consequence the slope of the CSL λ_c (crushing) becomes stiffer than λ (stable).

Although the described patterns of behavior slightly diverges from earlier findings reported by Yamamuro and Lade (1998), the characteristic behaviour illustrated in Figure 14 holds the essential concepts developed by the authors for silty sand materials.

3.2 State (void ratio/porosity) from seismic waves for assessment of liquefaction under critical state

For what has been referred, the importance of the evaluation of voids ratios (e), or porosity (n), by other means rather than undisturbed sampling—a difficult task in sensitive soils such loose sandy/silty soils—is a step ahead for a “clean” and reliable evaluation of state. With regard to empirical methods, an estimate of porosity could in principle be obtained from the initial shear modulus, G_{max} , using correlations that relate this parameter to the void ratio and the effective confining pressure, but these methods suffer from an intrinsic limitation due to the dependence of these empirical correlations on soil type, mineralogy and stress history. Similarly, the procedures used in coarse-grained soil deposits based on the estimate (from penetration tests) of the relative density have certain limitations, since they are affected by an uncertainty that is difficult to quantify, and they require independent measurements of e_{min} and e_{max} . Foti et al. (2002) proposes a novel procedure for determining porosity in fluid-saturated porous media from measured shear and dilatational (compression) wave velocities. The authors resume the method as a development of the theory of linear poroelasticity in the low-frequency limit, considering the fluid-saturated porous medium as a closed (undrained) system with the pore fluid moving in phase with the soil skeleton. The method presented by Foti et al. (2002) determines porosity of the in fluid-saturated media from the measured values of V_s and V_p . The method is based on the application of Biot’s theory under the assumption that no relative movement occurs in the porous medium between the solid and the fluid phases. This condition is considered to be fulfilled at low frequencies: that is, if the saturated porous medium is excited at

frequencies less than f_c , a characteristic frequency, defined by:

$$f_c = \frac{n \cdot g}{2 \cdot \pi \cdot k}$$

in which k is the coefficient of permeability of the medium, and g is the acceleration due to gravity. The lowest characteristic frequency is that associated with gravelly soils (70 Hz).

The value of porosity can be determined from the following relation:

$$n = \frac{\rho_s - \sqrt{(\rho_s)^2 - \frac{4 \cdot (\rho_s - \rho_f) \cdot K_f}{V_p^2 - 2 \cdot \left(\frac{1 - \nu_s}{1 - 2 \cdot \nu_s} \right) \cdot V_s^2}}}{2 \cdot (\rho_s - \rho_f)}$$

where, ρ_s and ρ_f is the Poisson ratio of the soil particles and the pore fluid, respectively, K_f is bulk modulus of the pore fluid, ν_s is the Poisson ratio of the soil skeleton and V_p and V_s the compression and shear velocities (measured experimentally). The values of K_f , ρ_s and ρ_f are physical constants that assume standard numerical values (Carmichael, 1989—some typical values in Foti et al. 2002) and ν_s is a priori unknown, but its range of variability is limited to 0.10–0.40 (Salem 2000).

The method has been successfully applied to estimate porosity at diverse sites (Foti et al. 2002, Foti Lancellota 2004; Arroyo et al. 2007) where cross-hole seismic data were available, the results showing very good agreement between the values of porosity predicted by the theory and those measured in the laboratory from undisturbed samples. Recently this has been applied to tailing materials (Jamiolkowski 2012) with utmost practical interest. This will be presented below in this text.

3.3 Evaluation of saturation level from *P*-waves velocities as to define the highest sensitive zone

From the two secondary factors that condition the uprising of the liquefaction risk, porosity was already discussed above, while saturation will be hereby analysed, being this factor a decisive condition for the development of more or less high pore pressures increments during a transient loading process.

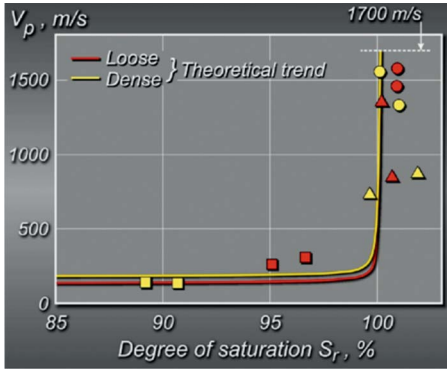
The important factor of guaranteeing complete saturation when dealing with remoulded soils for laboratory characterisation of cyclic mobility and/or liquefaction triggering has been emphasised by several authors (e.g. Viana da Fonseca et al. 2011). This problem of having an underestimation of this

risk has been addressed by different authors. Sherif et al. (1977), Chaney (1978), Yoshimi et al. (1989) have revealed that in laboratory tests the liquefaction resistance of sands depends strongly upon the degree of saturation, usually verified in terms of the pore pressure coefficient, B (Skempton 1954). At a specified cyclic stress ratio, the number of cycles causing liquefaction was found to increase substantially with decreasing values of B (Ishihara et al. 2001; Yang & Sato 1998, 2001; Vieira Faria et al. 2006).

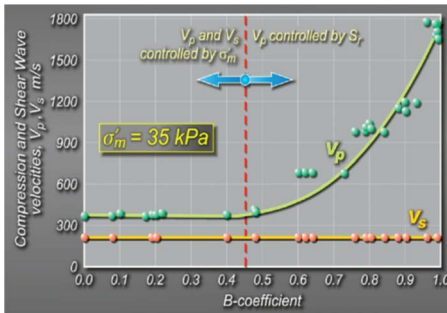
The use of the B -value test to determine the in situ state of saturation is sometimes difficult, and much influenced by compliance errors. However, it has been recognised that the velocity of compression waves (P -waves), V_p , is a clear sign of the identification of the water level, and the full saturation. The effectiveness of the use of V_p and Poisson's ratio ν in identifying in situ partially saturated zones has been demonstrated by a borehole array site (Yang & Sato 2001) and in zonation of highly heterogeneous residual soils masses, above and below water, with geophysical techniques (Viana da Fonseca et al. 2006).

There are even proposals that try to index the liquefaction resistance of a specific sand and its V_p to allow more significant interpretations and applications. As an example, Yang (2002) proposed an empirical function between the liquefaction resistance and B -value based on cyclic test data. There are theoretical relationships between the B -value and V_p , such as that based on Biot's theory for imperfectly saturated soils, considering the decrease in bulk modulus with the inclusion of air bubbles, proposed by Kokusho (2000). He presents some useful charts correlating B -value with V_p or ν . Yang also presents some of these charts, namely for Toyoura sand, and more recently Kiyoto et al. (2006) on Soma sand Valle-Molina (2006) in Ottawa sand (Figure 15a and b). Since V_p values clearly shows a high variation when the B -value varies from $B = 1.0$ and 0.8, it will be a most clear that they can be a very good index to detect imperfect or, "almost" full saturation—an ultimate condition for the sharp increase of liquefaction potential. Indeed, as presented by Kokusho (2000), for V_p larger than 90% of V_p of water, a B -value of 0.95 or greater should be expected.

There are now available explicit relations between the liquefaction resistance of sands and other soils and its P -wave velocity. These come from theoretical relationship between the value of B and the P -wave velocity into an empirical function relating the liquefaction resistance to B , established based on laboratory test data (Yang 2002). This allows to evaluate the in situ liquefaction resistance conditioned by saturation measuring P -wave velocity (Figure 16).



(a)



(b)

Figure 15. Relationship between V_p velocity and B -value for: (a) Soma sand (Kiyoto et al. 2006); (b) Ottawa sand (Valle-Molina 2006)—(Jamiolkowki, 2012. courtesy of the author).

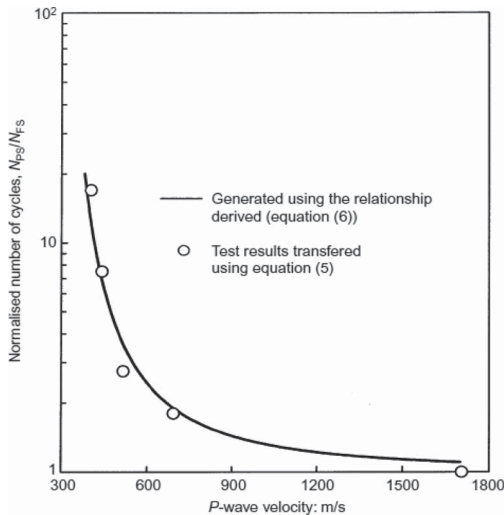


Figure 16. Normalised number of cycles for liquefaction as a function of P -wave velocity—sand with $D_r = 60\%$ (Yang 2002).

4 CASE-HISTORIES

4.1 Failures on tailing dams finally associated to static liquefaction dam

Davies et al. (2002) emphasizes that there was at this time limited mention of static liquefaction in regulatory literature and a good portion of the publications that refer to static liquefaction either do not explain the phenomenon being referred to or use the term as an explanation for any non-seismically triggered flow failure with no other common failure mechanism. This is still true in a large number of designers, who do not clearly recognize this mechanism. Davies et al. (2002) states that the fact that many more tailings dams have not failed due to this mechanism is in part due to the designers taking measures to combat seismic loadings and have also unintentionally guarded against static liquefaction. However, designs in low seismic areas may not have this co-incident safeguard. Unfortunately, a number of tailings dam failures have been mislabeled with other failure modes only to eventually have static liquefaction correctly noted as the contributing mode of dam failure (e.g. Fourie et al. 2001).

4.2 The failure of Merriespruit gold tailings dam

Fourie and Papageorgiou (2001) describe how this failure in South Africa was unusual in that never before had occurred in such a catastrophic way in gold tailings dams (Fig. 17). The conventional thinking was that gold tailings would always exhibit dilative characteristics upon loading, primarily because of the method of deposition which allows significant consolidation to occur due to sun-drying, which was not the case, since the re-analysis of the relative state location of the deposited materials towards its (their) steady state line, which separates dilative from contractive behavior



Figure 17. The Merriespruit tailings dam failure of 1994, with destruction of the village (Fourie & Papageorgiou 2001).

upon undrained loading, proved to be on the contractive zone, therefore unstable.

The interesting study involved the study of four particle-size distributions of Merriespruit tailings to determine the influence of the percent finer than 75 mm on the position of the steady state line. As concluded, the tailings with the greater percentage of fines gave a steady state line that plotted above all the others, requiring a greater relative density to produce non-contractive behavior than for the low-fines tailings samples (Figure 18). The difficulty of defining a unique steady state line for a particular tailing material was illustrated and it was recommended that error bands be assigned to any steady state line.

So exploring whether the in situ material can be at void ratios above the representative steady state line of the tailings (for relevant values of mean effective stress) and thus in a metastable or potentially liquefiable state, is critical. Therefore, the highly prospective possibility to occur static liquefaction in such projects, directly resulting in the catastrophic flow slide, demands for a thor-

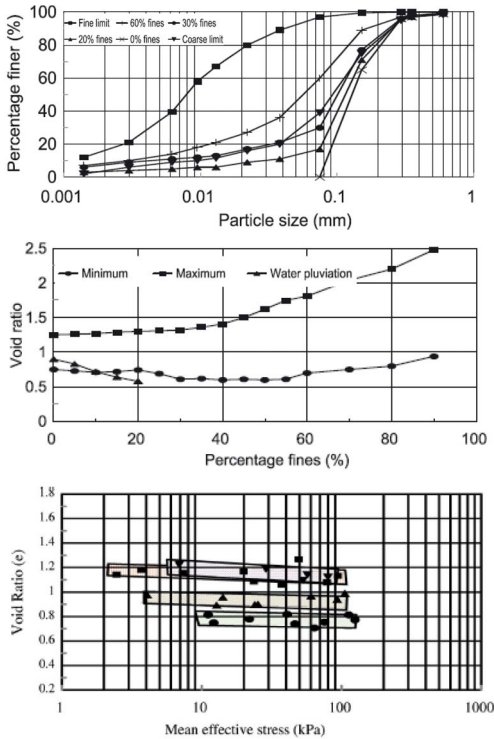


Figure 18. Particle-size distributions of Merriespruit tailings, variation of maximum and minimum void ratio with fines and distinct steady state lines from undrained triaxial compression tests on specimens exhibiting contractive behavior defining confidence zones based on state (adapted of Fourie & Papageorgiou 2001).

ough methodology of laboratory studies for the “good” evaluation of these critical (steady) state loci and subsequent continuous control the state parameter, which is obviously possible with in situ testing techniques.

In another paper, Fourie et al. (2001), describe how void ratios obtained from undisturbed samples taken during the post-failure investigation compared with those steady state lines have shown that an appreciable percentage of the specimens were likely to have been contractile. They concluded that a large volume of tailings was in a metastable state in situ and overtopping and erosion of the impoundment wall exposed this material, resulting in static liquefaction of the tailings and a consequent flow failure.

Five piezocone tests were carried out at various locations around the dam as part of the post-failure investigation were—Wagener et al. (1998), cited by the authors—and two are included in Figure 19.

The piezocone used in South Africa, at that time, did not include a friction sleeve, and results were only obtained for end resistance and pore-water pressure. Still, the profiles of end resistance q_c and pore pressure u_c for this latter test, revealed that the tailings at this location were very poorly consolidated, with dynamic pore pressures in excess of 300 kPa and cone resistance values of only 500 kPa at depths of as much as 14 m below the tailings surface. The graph on the right side in Figure 19, which is a profile of end resistance and pore pressure for the test conducted to the west of the breach and on the middle berm, shows end resistance values between depths of about 2 and 10 m which are significantly lower than those in any of the other three piezocone profiles measured on the middle and upper berms (Fourie et al. 2001). At a depth of 8.5 m, for example, the cone

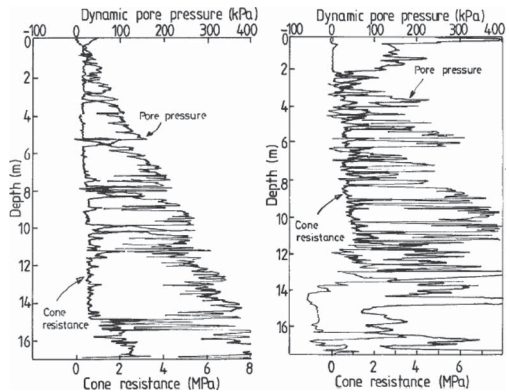


Figure 19. Results of post-failure piezocone tests conducted in Merriespruit dam adjacent to the decant facility and west of the breach on the middle berm (after Wagener et al. 1998).

resistance was only approximately 500 kPa. The authors deduced the undrained shear strength s_u , using the conventional the following equation:

$$s_u = \frac{q_c - \sigma_{v0}}{N_{kt}}$$

being N_{kt} an empirical cone factor analogous to the bearing capacity factor N_γ , with a “typical” value of 15, for normally consolidated clay deposits (Senneset et al. 1989), but since Tailings are likely to drain much more rapidly than a normally consolidated clay, being thus very difficult to measure a truly undrained shear strength, the piezocone is likely to overestimate the undrained shear strength (since some consolidation and thus increase in effective stress might occur in the vicinity of the advancing probe). Still, for mine tailings, which usually have nonplastic fines, Fourie et al. (2001) suggest that a N_{kt} value of 15 may be a good approximation and present some other values for mine tailings reported in the literature are summarized in Table 1, that tend to a little bit smaller than that reference, eventually due to that partial drainage.

Fourie et al. (2001)—citing Wagener et al. (1998)—refer that from the post-failure investigations carried out after Merriespruit tailings dam failure of 1994 it was concluded that there was indeed poorly consolidated material in the slope of the tailings dam and this material could be expected to flow in the event of disturbance or a removal of support.

4.3 The successful development of Zelazny Most in South-West Poland, with the strict control of the evolution of the tailings from in situ tests results

Jamiolkowski et al. (2010) describe a reference case-history of the world largest copper tailings disposal at Zelazny Most in South-west Poland, close to the borders with the Czech Republic and Germany, Figure 20. In this lecture the geological features of the area and the geotechnical aspects of the design and construction. But, it is the geotechnical characterization of the tailings and of the foundation soils that are most interesting to this workshop.

Table 1. Reported values of the empirical cone factor N_{kt} for mine tailings (after Fourie et al. 2001).

Tailings	N_{kt}	Reference
Copper	15.5 ± 4.5	Mlynarek et al. 1994
Unknown	9–12	East et al. 1988
Uranium	15–19	Larson & Mitchell 1986
Unknown	10.4	East & Ulrich 1989

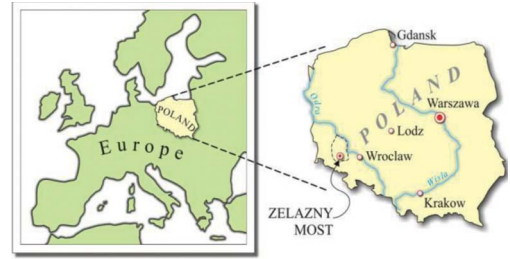


Figure 20. Zelazny Most copper tailings disposal location in Poland (Jamiolkowski et al. 2010).



Figure 21. Tailings disposal, aerial view.

Zelazny Most is the largest tailings dam in Europe, and it is among the largest upstream tailings dams in the world. Sensitive subjects such as shear strength of the involved materials, in what respects the mining-induced seismicity and the stability of the ring-dam that confines the tailings, are described and some of the most adapted techniques and analyses are discussed.

The Zelazny Most mining system, for extraction of copper since in 1972, involves a 480 Mm³ of tailings stored in the disposal area, and the maximum height of the dam is close to 60 m. An aerial view of the Zelazny Most disposal is shown in Figure 21.

From the geotechnical issues involved in their design and construction, the possibility of flow liquefaction of the stored tailings is a phenomenon which has been responsible for the collapse of several tailings dams, and which frequently involve casualties. Another issue of concern for the designers of tailings dams is the stability of the dams, which depends on the height of the dam and the mechanical behaviour of the foundation soils.

The Zelazny Most tailings disposal is situated on a high plasticity Pliocene clay with shear surfaces ruled by a shear strength close to residual values which constitute a challenge stability analysis of the dam. Considering the magnitude and extent of the Zelazny Most scheme (the ring-dam is almost

15 km in circumference), and its importance for the continuing operation of the mining operations, the owner (KGHM) appointed a four-member International Board of Experts (IBE): Prof.s M. Jamiolkowski, W.D. Carrier, R.J. Chandler, K. Hoeg, W. Swierczynski and W. Wolski who have reported this case-history in the 1st Za Chieh-Moh Distinguished Lecture (Jamiolkowski et al. 2010).

The production of this industrial plant gives rise to a large portion waste mineral material (tailings). The tailings are transported hydraulically from the mine beneficiation plant to a disposal area, referred to as a tailings pond. These material are deposited, the water decanted and re-cycled back to the beneficiation plant. The tailings pond includes a dam to retain the tailings, depending on the local topography, which is the case of Zelazny Most, as in other disposals, similar to the scheme included in Figure 22 (Jamiolkowski et al. 2010). It is being raised by the upstream method, Figure 2, being these tailings completely surrounding the pond. A plan view is shown in Figure 23.

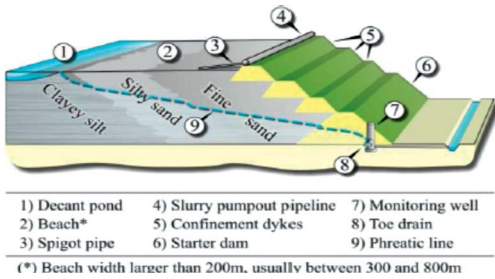


Figure 22. Schematic cross-section of Zelazny Most tailings disposal (Jamiolkowski et al. 2010).

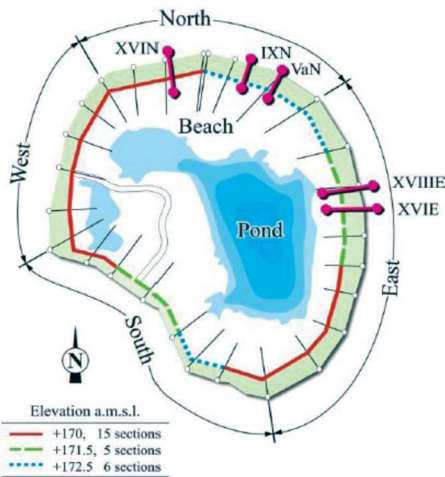


Figure 23. Dams elevations and relevant cross-sections (Jamiolkowski et al. 2010).

Presently, the crest of the dam is at approximately elevation 170 m above sea level (asl). The height of the dam above the downstream natural grade varies from approximately 22 to 60 m. There are approximately 480 Mm³ of tailings presently stored and the end of deposition is projected to occur in 2042, with a total volume of approximately 933 Mm³. The deposition of tailings began in 1977, with a rising rate of approximately 1.25 to 1.5 m/yr, with a downstream slope of approximately 3.5 horizontal to 1 vertical.

The beach (the distance from the crest to the edge of the pond) has been maintained at a minimum distance of 200 m. With this practice that have the effect of displacing the softer, weaker slimes farther inward and produce a thick, strong, dilative shell. Finally, as described in Jamiolkowski et al. (2010), draining systems have depressed the phreatic surface, with the stability of the dam being controlled by the foundation soils, instead of being controlled by the tailings (Figure 24).

The observational method has always been a major concern in design and operation of tailings dam. In order to monitor the deposition of the tailings and the performance of the Zelazny Most tailings dam, there are approximately 300 surface marks for measuring horizontal and vertical movements. In addition, a total station with 23 micro-mirrors has recently been installed to more closely monitor one particular section of the dam. There are also approximately 1800 piezometers, of which 870 piezometers have their tips in the tailings, 830 in the foundation soils, and 100 in the starter dam. Finally, there are 42 deep inclinometers. In the future, the dam may also be monitored by means of satellite radar interferometry.

The important factor of stability of the foundation soils included the following aspects of geotechnical characterization: (1), to establish the foundation geology; (2), to determine strength properties for limit equilibrium stability analyses; and (3), to estimate the in-situ stress state, stress-strain behavior, and undrained and effective stress strength parameters for finite element analysis. According to Jamiolkowski et al. (2010), this has been done by sampling from downstream of the toe of the dam (the “fore-field”) so as far as possible to be sure that the soil is unaffected by the

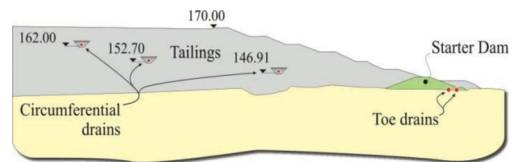


Figure 24. East Dam, location of the circumferential drains.

construction of the dam. This will not be developed in the context of this work, since the purpose is to describe what has been carried out over the last twenty years in an attempt to achieve a comprehensive and reliable geotechnical characterisation of the tailings.

In Jamiolkowski et al. (2010) paper, there is an important reference to the works of Lipinski (2000; 2005), describing the characterisation of the tailings used in this project. Coarse tailing from the Rudna and Lubin Mines are used to raise the dam, whilst the much finer tailings from the Polkowice Mine are deposited hydraulically directly in the pond. The range of particle size distribution of the Rudna and Lubin tailings were investigated by Lipinski (2000, 2005), and are shown in Figure 25 together with their mineralogical composition and the range of specific gravity, G_s . The values of IP of the more plastic fine tailings do not exceed 12; many samples are non-plastic.

Characterisation was made by recurring to using in-situ tests, due to the difficulties of having good undisturbed samples. A significant number—hundreds in accordance to Jamiolkowski et al. 2010—of static cone penetration tests (CPT and CPTU), have been carried out. Some of these cone resistance (q_c) profiles, measured during CPTU tests on the beach of the East Dam, at various distance from the dam crest, are shown in Figure 26. The authors comment the variability of the q_c values with depth resulting from spigotting, reflected in the cone resistance decreasing with increasing distance from the dam crest, is attributed to the

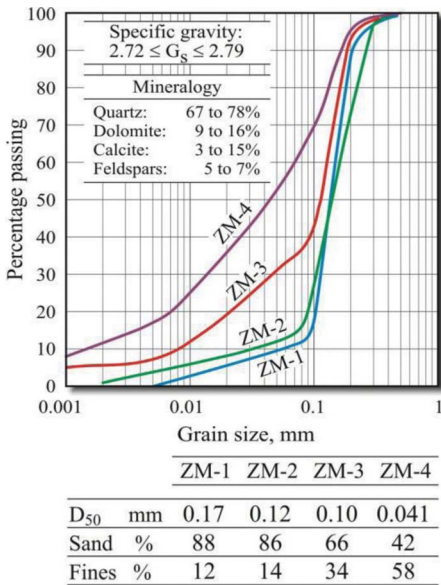


Figure 25. Tailings grain size distribution (Jamiolkowski et al. 2010).

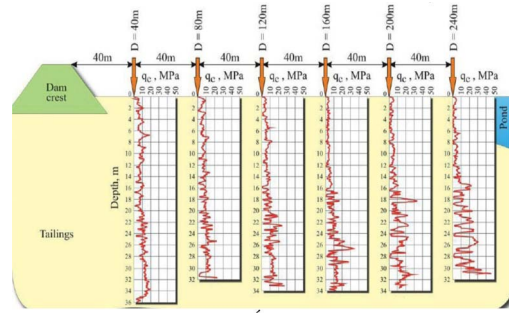


Figure 26. Tailings grain size distribution (from Jamiolkowski et al. 2010).

increase in fine content as the test location gets closer to the pond.

Similar comments are made regarding the results of two seismic Marchetti's flat dilatometer [S-DMT] tests (Marchetti et al. (2008; 2009) run on the beach of the East Dam at distances of 40 and 200 metres from the dam crest, as shown in Figure 27.

As revealed above, the use of geophysical methods for mechanical characterization of the tailings, specially in the light of a critical state approach is highly recommendable for the evaluation of the dam stability. The necessity of having the information on the distribution of the void ratio (deduced from porosity) in the tailings' masses will enable to mapping risk zones if a sustained definition of patterns of critical state loci can be attained from preliminary studies over the tailings used in this project (Figure 27).

Several cross-hole (CH) and down-hole (DH) tests were carried out to measure seismic compression (V_p) and the shear wave (V_s) velocities. These were complemented with a number of seismic static cone penetration tests (S-CPTU) and, still, the above mentioned seismic dilatometer tests (S-DMT's), during which V_s was measured. In all seismic tests the wave velocity was measured using two receivers, allowing the assessment of V_p and V_s by the true time interval method.

The results of seismic wave velocity measurements within the tailings were explored for (i) the evaluation of the in-situ void ratio (e_0) as function of V_p and V_s under the formula of Foti et al. (2002)—see above; (ii) the assessment of the saturation line and the spatial distribution of fully saturated tailings based on the measured V_p values; and, (iii) the quantitative assessment of the susceptibility of the saturated (or nearly saturated) tailings to static liquefaction, based on the value of V_s . Some of Ch tests results are presented in Figure 28.

The values of V_s (VH) and V_s (HH) suggest (Figure 28) that the tailings have very limited initial (i.e. small strain) anisotropy.

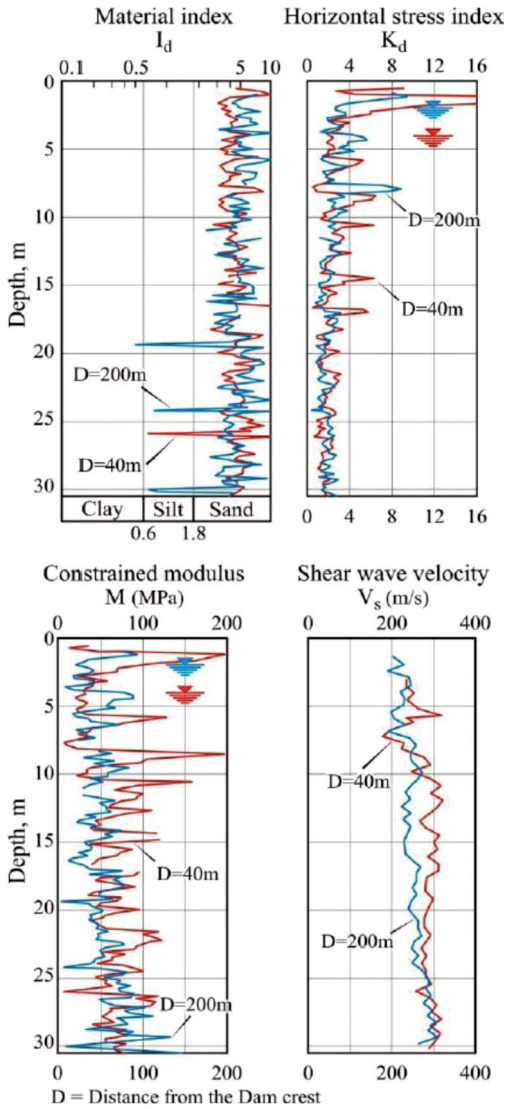


Figure 27. East Dam, results of two S-DMT's (from Jamiolkowski et al. 2010).

The V_p values confirm their usefulness as a sensitive indicator of the depth at which the tailings become fully saturated; see Valle Molina (2006). Assuming that saturation coincides with the depth at which the V_p values exceeds 1500 m/s, on the cross-section considered the saturation line can be identified as occurring at depths of 28 m ($D = 40.6$ m), 20 m ($D = 132$ m) and 9 m ($D = 217$ m), D being the distance from the dam crest. Once the position of the saturation line has been identified, the values of e_0 can be estimated using the formula of Foti et al. (2002).

These calculations were carried out for a series of 10 cross-hole tests, which averaged values are

plotted in Figure 29, together with the standard deviation of each of the averaging (Jamiolkowski 2012). This low error levels reveal the high reproducibility of such wave measurements.

In another analysis, Jamiolkowski presents the values of V_s and V_p of saturated tailings used in the calculation of e_0 for the six tests performed in 1997, and the last values computed from those cross-hole test results (Figure 30).

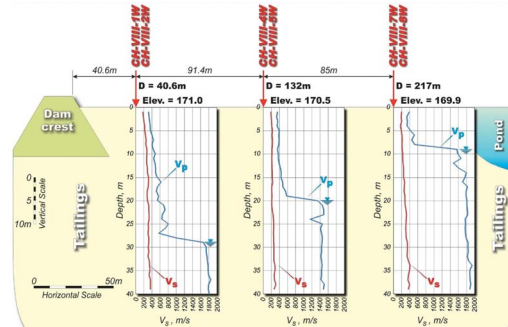


Figure 28. West Dam—Section VIII, cross-hole tests results (Jamiolkowski 2012—courtesy of the author).

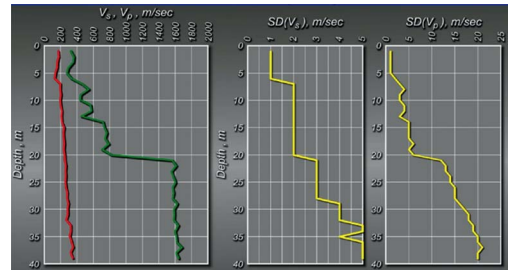


Figure 29. West Dam—200 m from the dam crest, cross-hole tests results (average V_s and V_p values and standard deviations (Jamiolkowski, 2012—courtesy of the author).

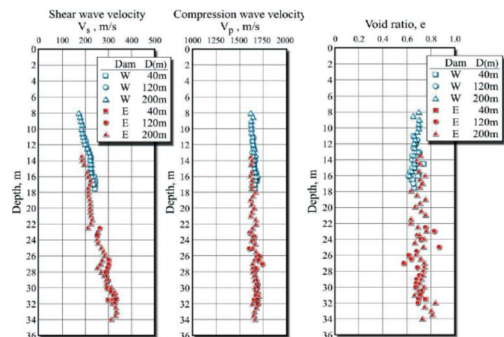


Figure 30. East Dam, seismic wave velocity of saturated tailings and void ratio—CH tests (Jamiolkowski et al. 2010).

It can be seen in Figure 29, once the position of the saturation line has been identified, the values of e_0 can be estimated using the formula of Foti et al. (2002), using seismic test results, in the present cases by recurring to cross-hole.

Jamiolkowski et al. (2010) remind that consolidated undrained triaxial, compression and extension, on isotropically and anisotropically consolidated specimens (TX-CIU; TX-CAU tests), were essential to define the critical state loci, being this performed on specimens reconstituted using the ‘under-compaction’ method (Ladd 1974, 1978) with a few further tests using pluvial deposition and slurry sedimentation (Lipinski 2000). All the reconstituted samples, except for a few prepared by slurry sedimentation, exhibited a pronounced susceptibility to flow failure. A thorough definition of the state condition in relation to more or less susceptible areas in relation to critical stress, would allow for the evaluation of the level of risk towards liquefaction triggering (see Figure 13). Still, in the light of the importance of this project there was a serious concern in relying on the behavior of the laboratory tested reconstituted samples. Therefore, in 1993, it was decided to attempt “undisturbed” sampling (using thin-wall samplers, 70 mm in diameter and 140 mm in height), of the tailings in hand-dug pits located in the beach at varying distances from the dam crest (Jamiolkowski et al. 2012). Although the adopted sampling method does not guarantee entirely undisturbed specimens, the tests showed a very different behavior of tailings during undrained shearing from that obtained in the earlier series of tests. All the undisturbed specimens initially exhibited contractive behaviour, passing through the point of phase transformation (Ishihara 1993) and then exhibiting continuous dilation as shown in Figure 31. More recent tests have been executed with similar results.

It is interesting to note that a comparison between the behavior of undisturbed and reconstituted specimens was made in the light of former approaches (Hight 2000; Ferreira et al. 2004, 2011; Landon et al. 2007) based on comparable values of the initial shear modulus, G_0 , deduced from the value of V_s , measured in situ and on triaxial tests using bender elements. Table shows the results of the series of tests carried out in 1998 (Jamiolkowski et al. 2010). It is seen that not only is the strength of the “undisturbed” samples greater, but that the values of G_0 are also constantly higher. It seems that specimens taken from the trial pits in the beach, despite the non-ideal sampling procedure, have preserved, at least partially, the in-situ soil fabric of the tailings.

It is interesting to present the parametrical analysis of Monaco & Marchetti (2007) over results

obtained on DMT and Cross-Hole tests (CHT), from which some are plotted in Figure 32.

Considering the possibility of occurring seismic actions, Monaco & Marchetti (2007) plotted the range of values obtained for such profiles—Figure 32—and situated them in the liquefaction risk assessment charts of Figures 6 and 8a, where Cyclic Resistance Ratio (CRR) is defined, respectively, in terms of V_{s1} and K_p . These ranges are signaled in thick lines in the abscissa axis of Figure 33.

They have also plotted the limit values for V_{s1} and K_p , for a very strong earthquake action $M_w = 7.5$ which would be associated to the values of $V_{s1} = 215$ m/s and $K_p = 5.5$ (Maugeri and Monaco 2006), for clean sands. In this example (Figure 33) the materials of Zelazny Most tailing dam, represented by the example in Figure 32, would give

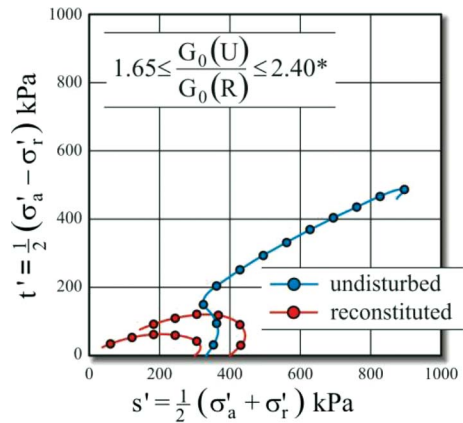


Figure 31. Example of undrained triaxial compression tests on tailings (adapted from Jamiolkowski et al. 2010).

Table 2. Undrained triaxial tests results on saturated tailings (Jamiolkowski et al. 2010).

L (m)	FC (%)	e_0 (-)	Test* type	B-range (-)	$(G_0)_1$ (bar)	$\frac{(G_0)_1 U}{(G_0)_1 R}$
40	22	0.811	U	0.968 to 0.991	849	1.23
		0.809	R	0.976 to 0.996	691	
120	24	0.806	U	0.950 to 0.987	851	1.20
		0.821		0.971 to 0.994	709	
200	28	0.810	U	0.967 to 0.995	857	1.27
		0.808	R	0.980 to 0.995	674	

(*) TX-CAU-CL, σ'_{vc} : 50, 250 and 500 kPa, $\frac{\sigma'_c}{\sigma'_{vc}} = 0.5$

- L = Distance from the dam crest
- $(G_0)_1 = G_0$ at $\sigma'_m = 1$ bar
- FC = Fine content, low plasticity silt
- U = Undisturbed specimens
- R = Reconstituted specimens

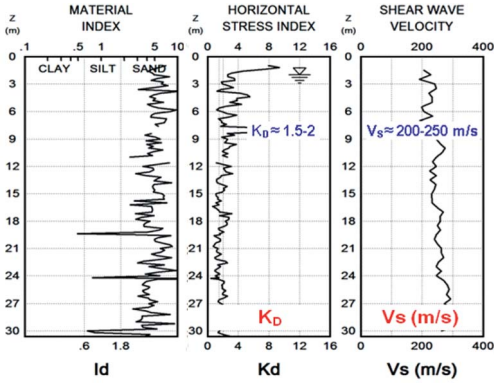


Figure 32. Profiles of K_D and I_D (DMT parameters) and V_s , shear wave velocities from CHT (Jamiolkowski et al. 2010).

an indication that “no liquefaction” would occur if V_{s1} values were considered (mostly > 215 m/s), while, for the same earthquake, under K_D values ($\approx 1.5-2$), there is an indication that liquefaction may occur above a certain seismic stress level (high CSR). Looking at this data, even for lower values of action (smaller values of CSR) the indications of V_s would point to stability, while K_D point in the opposite direction.

Therefore, preliminary comparisons indicate that methods based on V_s and K_D would provide, in general, different estimates of CRR, for what Monaco & Marchetti (2007) propend to give greater weight to CRR by K_D since it may have higher sensitivity to stress history and agying, which greatly increase liquefaction resistance.

5 CONCLUDING REMARKS

The fundamentals of the liquefaction phenomena were summarized with the purpose of stressing the importance of the in situ tests for deriving the crucial parameters that reveal the state condition and therefore the risk for instability. Liquefaction is a term most often associated with seismic events. However, mine tailings impoundments have demonstrated more static liquefaction events than seismic induced events. The summary of the fundamentals includes particular emphasis on static liquefaction.

Several static liquefaction case histories are described to demonstrate various ways in which this failure mechanism has manifested itself. From an understanding of the fundamentals and the lessons learned from the case histories, basic guidelines to minimize the concern for tailings impoundments were presented focusing the great help on specific in situ tests, thoroughly interpreted.

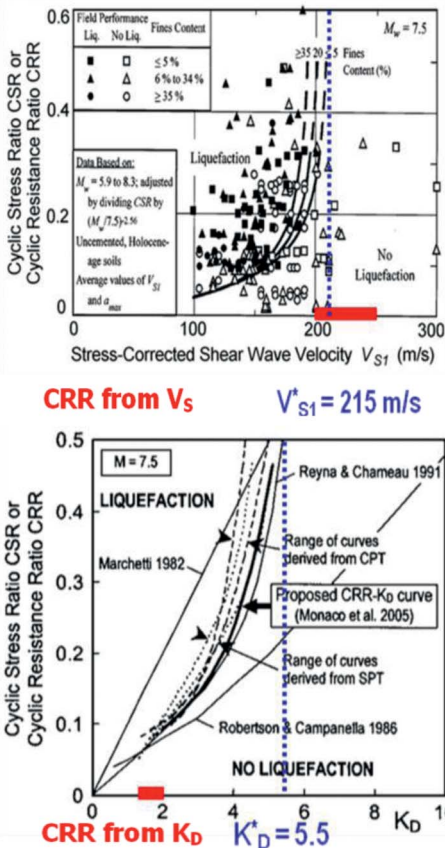


Figure 33. Profiles of K_D and I_D (DMT parameters) and V_s , shear wave velocities from CHT (Jamiolkowski et al. 2010).

ACKNOWLEDGEMENTS

This work was developed under the research activities of CEC (University of Porto), supported by multi-annual funding from FCT (Portuguese Science and Technology Foundation), specifically the research project PTDC/ECM/103220/2008, financed by QREN from the European Communion (UE/FEDER), through the Operational Program for Competitive Factors—COMPETE.

REFERENCES

Andrade, J.E. 2009. A predictive framework for liquefaction instability, *Geotechnique*, 59(8): 673–682
 Andrus, R.D. & Stokoe, K.H., II. 2000. Liquefaction resistance of soils from shear-wave velocity, *Journal*

- of *Geotechnical and Geoenvironmental Engineering*, ASCE, 126(11): 1015–1025.
- Andrus, R.D., Stokoe, K.H., II & Juang, C.H. 2004. Guide for Shear-Wave-Based Liquefaction Potential Evaluation. *Earthquake Spectra*, 20(2): 285–305.
- Arango, I., Lewis, M.R. & Kramer, C. 2000. Updated liquefaction potential analysis eliminates foundation retrofitting of two critical structures. *Soil Dynamics Earthquake Engrg.*, 20: 17–25.
- Arroyo, M., Ferreira, C. & Sukolrat, J. 2007. Dynamic measurements and porosity in saturated triaxial specimens. *Soil Stress-Strain Behavior: Measurement, Modeling and Analysis*. Ling et al. (Ed). Springer, pp. 537–546.
- Baldi, G., Bellotti, R., Ghionna, V., Jamiolkowski, M. & Pasqualini, E. 1985. Penetration Resistance and Liquefaction of Sands. Proc. 11th ICSMFE, San Francisco, Vol. 4, pp. 1891–1896.
- Bedin, J. 2010. *Study of the Geomechanical Behavior of Tailings*. Ph.D. thesis in Civil Engineering, UFRGS, Porto Alegre, Rio Grande do Sul.
- Bedin, J., Schnaid, F., Viana da Fonseca, A. & Costa Filho, L. de M. 2011. Gold tailings liquefaction under critical state soil mechanics. *Géotechnique*. 62(3): 263–267.
- Been, K. & Jefferies, M.G. 1985. A state parameter for sands. *Géotechnique*, 35(2): 99–112.
- Blight, G. 2009. *Geotechnical Engineering for mine waste storage facilities*. CRC Press, Taylor & Francis Group.
- Borja, R.I. 2006. Condition for liquefaction instability in fluidsaturated granular soils. *Acta Geotechnica*. 1(4): 211–224.
- Campbell, D.L. & Fitterman, D.V. 2000. Geoelectrical methods for investigating mine dumps. Proc. Fifth International Conference on *Acid Rock Drainage* (ICARD 2000), Denver, Colorado. Society for Mining, Metallurgy, and Exploration, Inc., Vol. II, p. 1513–1523.
- Carmichael, R.S. 1989. *Practical handbook of physical properties of rocks and minerals*. Florida, USA, Boca Raton: CRC Press.
- Carrera, A., Coop, M.R. & Lancellotta, R. 2011. The Influence of grading on the mechanical behaviour of Stava tailings. *Géotechnique*, 61(11): 935–946.
- Carrier, W.D. 2003. Stability of tailing dams. XIX Conference of Geotechnics of Turin on slope stability and stabilization, Turin, Italy.
- Casagrande, A. 1936. Characteristics of cohesionless soils affecting the stability of earth fills, J. Boston Society of Civil Engineers, Vol. 23, 257–276.
- Casagrande, A. 1976. Liquefaction and cyclic deformation of sands, a critical review. *Harvard Soil Mechanics Series* No. 88, Harvard Univ. Cambridge, Massachusetts.
- Castro, G. 1975. Liquefaction and cyclic mobility of saturated sands. *Journal of Geotechnical and Geoenvironmental Engineering*, ASCE, 101(6): 551–569.
- Chandler, R.J. & Tosatti G. 1995. The Stava tailings dams failure, Italy, July 1985. Proc. *Instn Civ. Engrs., Geotech. Engrg.*, Vol. 113, 67–79.
- Chaney, R. 1978. Saturation effects on the cyclic strength of sand. Proc. *ASCE special conference on earthquake engineering and soil dynamics*, 342–359.
- Coop, M.R. & Lee, I.K. 1993. The behaviour of granular soils at elevated stresses. *Predictive Soil Mechanics*, Thomas Telford, London: 186–198.
- Davies, M. McRoberts, E. & Martin. T. 2002. Static liquefaction of tailings—fundamentals and case histories. In *Proceedings of Tailings Dams 2002*, ASDSO/USCOLD, Las Vegas.
- Doanh, T., Ibraim, E. & Matiotti, R. 1997. Undrained instability of very loose Hostun sand in triaxial compression and extension. Part 1: Experimental observations. *Mech. Cohesive-Frictional Mater.* 2(1): 47–70.
- Dubujet, Ph. & Doanh, T. 1997. Undrained instability of very loose Hostun sand in triaxial compression and extension. Part 2: Theoretical analysis using an elastoplasticity model. *Mech. Cohesive-Frictional Mater.* 2(1): 71–92.
- Eslaamizaad, S. & Robertson, P.K. 1996. A Framework for In-situ determination of Sand Compressibility. *49th Canadian Geotechnical Conference*; St John's Newfoundland.
- Ferreira, C., Mendonça, A.A. & Viana da Fonseca, A. 2004. Assessment of sampling quality in experimental sites on residual soils from Porto granite. Proc. *9th Portuguese Conf. on Geotechnics*. Vol. 1, 27–38. SPG, Lisbon.
- Ferreira, C., Viana da Fonseca, A. & Nash, D. 2011. Shear wave velocities for sample quality assessment on a residual soil. *Soils and Foundations*. 51(4): 683–692.
- Foti, S., Lai, C. & Lancellotta, R. 2002. Porosity of fluid-saturated porous media from measured seismic wave velocities. *Géotechnique*, 52(5): 359–373.
- Foti, S. & Lancellotta, R. 2004. Soil porosity from seismic velocities. *Géotechnique*, 54(8): 551–554.
- Fourie, A.B., Blight, G.E. & Papageorgiou, G. 2001. Static liquefaction as a possible explanation for the Merriespruit tailings dam failure. *Canadian Geotechnical Journal*, 38: 707–719.
- Fourie, A.B. & Papageorgiou, G. 2001. Defining an appropriate steady state line for Merriespruit gold tailings. *Canadian Geotechnical Journal*, Vol. 38: 697–706. *On Tailings and Mine Waste '98*, Colorado State University, Fort Collins, January 1998, pp. 925–952.
- Grasso, S. & Maugeri, M. 2006. Using K_D and V_s from seismic dilatometer (SDMT) for evaluating soil liquefaction. Proc. 2nd International Flat Dilatometer Conference, pp. 281–288.
- Hardin, B.O. 1978. The nature of stress-strain behavior of soils. *Geotechnical Div. Specialty Conf. on Earthquake Engineering and Soil Dynamics Pasadena*, California. ASCE, 1: 3–90.
- Hardin, B.O. & Richart, F.E. Jr. 1963. Elastic wave velocities in granular soils. *Journal of Soil Mechanics and Foundation Division*, ASCE, 89(1): 33–65.
- Hazen, A. 1920. Hydraulic fill dams. *Transactions*, American Society of Civil Engineers, Vol. 83, pp. 1713–1745.
- Hepton, P. 1988. Shear wave velocity measurements during penetration testing. Proc. *Penetration Testing in the UK*, ICE, 275–278.
- Hight, D.W. 2000. Sampling methods: Evaluation of disturbance and new practical techniques for high quality sampling in soils. Proc. *7th Portuguese Conf. on Geotechnics*, Porto. Vol. 1, pp. 1–35. SPG, Lisbon.

- Huang, A.B. & Ma, M.Y. 1994. An analytical study of cone penetration tests in granular material. *Canadian Geotechnical Journal*, 31(1): 91–103.
- Idriss, I.M. & Boulanger, R.W. 2006. Semi-empirical procedures for evaluating liquefaction potential during earthquakes. *Soil Dynamics and Earthquake Engineering*, Vol. 26, 115–130.
- Ishihara, K. 1993. Liquefaction and flow failure during earthquakes. *Géotechnique* 53(3): 351–415.
- Ishihara, K., Tsuchiya, H., Huang, Y. & Kamada, K. 2001. Recent studies on liquefaction resistance of sand—effect of saturation. (*Keynote Lecture*). Proc. 4th Int. Conf. on Recent Advances in Geotechnical Earthquake Engineering and Soil Dynamics, San Diego, California.
- Iwasaki, T., Tatsuoka, F. & Takagi, Y. 1978. Shear moduli of sands under cyclic torsional shear loading. *Soils and Foundations*, 18(1): 39–56.
- Jamiolkowski, M. 2012. Role of Geophysical Tests in Geotechnical Site Characterization. *Victor de Mello Lecture*, Lisbon. To be published in *Soils and Rocks*. ABMS, S. Paulo.
- Jamiolkowski, M., Carrier, W.D., Chandler, R.J., Hoeg, K., Swierczynski, W. & Wolski W. 2010. The geotechnical problems of the second world largest copper tailings pond at Zelazny Most, Poland. 1st Za Chieh-Moh Distinguished Lecture. *Geotechnical Engineering Journal of the SEAGS & AGSSEA*. 41(1): 1–15 (ISSN 0046-5828).
- Jamiolkowski, M. & Lo Presti, D.C.F. 1998. “DMT research in sand. What can be learned from calibration chamber tests”. *1st Int. Conf. on Site Characterization ISC '98*, Atlanta. Oral presentation.
- Jefferies, M.G. & Been, K. 2006. *Soil Liquefaction—A critical state approach*. Taylor & Francis, ISBN 0-419-16170-8 478 pages.
- Jefferies, M.G. & Davies, M.P. 1993. Use of CPTU to estimate equivalent SPT N_{60} . *Geotechnical Testing Journal, ASTM*, 16(4): 458–468.
- Jendeby, L. 1992. Deep Compaction by Vibrowing. *Proc. Nordic Geot. Meeting NGM-92*, Vol. 1, 19–24.
- Kiyota, T., Sato, T., Koseki, J. & Tsutsumi, Y. 2006. Comparison of liquefaction properties of in-situ frozen and reconstituted sandy soils, *Geomechanics and Geotechnics of Particulate Media* (Hyodo et al. eds), Yamaguchi, Japan, 113–119.
- Kokusho, T. 2000. Correlation of pore-pressure B -value with P -wave velocity and Poisson's ratio for imperfectly saturated sand or gravel. *Soils and Foundations*, 40(4): 95–102.
- Kramer, S.L. 1996. *Geotechnical Earthquake Engineering*. Prentice Hall, Inc., Upper Saddle. 653 pp. New Jersey, USA.
- Ladd, R.S. 1974. Specimen preparation and liquefaction of sands. Technical Note. *Journal of Geotechnical and Geoenvironmental Engineering*, ASCE. 100(10): 1180–1184.
- Ladd, R.S. 1978. Preparing test specimens using undercompaction. *ASTM Geotechnical Testing Journal*, 1(1): 16–23.
- Landon, M.M., DeGroot, D.J. & Sheahan, T.C. 2007. Nondestructive sample quality assessment of a soft clay using shear wave velocity. *Journal of Geotechnical and Geoenvironmental Engineering*, ASCE. 133(4): 424–432.
- Lipinski, M.J. 2000. Undrained Response of Cohesionless Soils to Monotonic Loading. *Ph.D. thesis*, Technical University of Gdansk, Poland.
- Lipinski M.J. 2005. Evaluation of change in shear strength of Żelazny Most tailings material. Technical Report, Geoteko Ltd.
- Lo Presti, D.C.F. 1995. General report: Measurement of shear deformation of geomaterials in the laboratory. *Pre-failure Deformation of Geomaterials*. Shibuya, Mitachi & Miura (eds). Balkema, Rotterdam, Vol. 2, 1067–1088.
- Marchetti, S. 1980. In Situ Tests by Flat Dilatometer. *Jnl GED*, ASCE, 106(GT3), 299–321.
- Marchetti, S. 1982. Detection of liquefiable sand layers by means of quasi-static penetration tests. *Proc. 2nd European Symp. on Penetration Testing*, Amsterdam, Vol. 2, 689–695.
- Marchetti, S. 2010. Sensitivity of CPT and DMT to stress history and aging in sands for liquefaction assessment. *2nd International Symposium on Cone Penetration Testing*, Paper No. 3-50. CD-Rom or in: www.cpt10.com
- Marchetti, S. 2011. Discussion of “CPT-DMT Correlations” by P.K. Robertson. *Journal of Geotechnical and Geoenvironmental Engineering*, ASCE. 137(4): 441–442.
- Marchetti, S., Monaco, P., Totani, G. & Calibrese, M. 2001. The flat dilatometer (DMT) in soil investigations (ISSMGE TC16). Proc. Int. Conf. on *In-Situ Measurement of Soil Properties and Case Histories*, Bali, Indonesia, pp. 95–131.
- Marchetti, S., Monaco, P., Totani, G. & Marchetti, D. 2008. In situ tests by seismic dilatometer (SDMT). Vol. honouring J.H. Schmertmann, ASCE, GSP, Vol. 180, 292–311.
- Martin, G.K. & Mayne, P.W. 1997. Seismic Flat Dilatometer Tests in Connecticut Valley Varved Clay. *ASTM Geotech. Testing Jnl*, 20(3): 357–361.
- Martin, G.K. & Mayne, P.W. 1998. Seismic flat dilatometer in Piedmont residual soils. *Proc. 1st Int. Conf. on Site Characterization ISC'98*, Atlanta. Vol. 2, 837–843.
- Maugeri, M. & Monaco, P. 2006. Liquefaction Potential Evaluation by SDMT. *Proc. 2nd Int. Conf. on the Flat Dilatometer*, Washington D.C., 295–305.
- Mayne, P.W., Schneider, J.A. & Martin, G.K. 1999. Small- and large-strain soil properties from seismic flat dilatometer tests. *Proc. 2nd Int. Symp. on Pre-Failure Deformation Char.s of Geomaterials*, Torino. Vol. 1, 419–427.
- Middlebrooks, T.A. 1940. Fort Peck slide, with discussions by Messrs. J. Field, J.D. Justin, W. Gerig, A.J. Ryan, G. Gilboy, F.E. Fahlquist, I.B. Crosby & T.A. Middlebrooks, ASCE, *Transactions*, Paper No. 2144, 723–764.
- Mitchell, J.K., Lodge, A.I., Coutinho, R.Q., Kayen, R.E., Seed, R.B., Nishio, S. & Stokoe, K.H. 1994. Insitu test results from four Loma Prieta earthquake liquefaction site: SPT, CPT, DMT and shear wave velocity. Report No. UCB/EERC-94/04, Earthquake Engineering Research Center, University of California, Berkeley.

- Monaco, P., Marchetti, S., Totani, G. & Calabrese, M. 2005. Sand liquefiability assessment by Flat Dilatometer Test (DMT). *Proc. XVI ICSMGE*, Osaka. Vol. 4, 2693–2697.
- Monaco, P. & Marchetti, S. 2007. Evaluating liquefaction potential by seismic dilatometer (SDMT) accounting for aging/stress history. *Proc. 4th International Conference on Earthquake Geotechnical Engineering*, Thessaloniki, paper No. 1626, Springer.
- Monaco, P. & Schmertmann, J.H. 2007. Discussion of “Accounting for Soil Aging When Assessing Liquefaction Potential” by Leon et al. (in *Jnl GGE*, ASCE, 2006, 132(3): 363–377).
- Morgenstern N.R. & Küpper A. 1988. Hydraulic fill structures—a perspective. *ASCE Geotechnical Special Publication No. 21*, van Zyl & Vick (eds) Fort Collins Colo., 1–31.
- Moss, R.E.S., Seed, R.B. & Olsen, R.S. 2006. Normalizing the CPT for overburden stress. *Journal of Geotechnical and Geoenvironmental Engineering*, ASCE, 132(3): 378–387.
- Ohta, Y. & Goto, N. 1978. Empirical shear wave velocity equations in terms of characteristic soil indexes. *Earthquake Engrg. Struct. Dyn.*, 6: 167–187.
- Olson, S.M. & Stark, T.D. 2003. Yield strength ratio and liquefaction analysis of slopes and embankments. *Journal of Geotechnical and Geoenvironmental Engineering*, ASCE, 129(8): 727–737.
- Reyna, F. & Chameau, J.L. 1991. Dilatometer Based Liquefaction Potential of Sites in the Imperial Valley. Proc. 2nd nt. Conf. on *Recent Advances in Geotechnical Earthquake Engrg. and Soil Dynamics*, St. Louis, 385–392.
- Rix, G.J. & Stokoe, K.H. 1992. Correlations of initial tangent modulus and cone resistance. *Proc. Int. Symp. Calibration Chamber Testing*. Potsdam, New York: 351–362. Elsevier.
- Robertson, P.K. 1990. Soil classification using the cone penetration test. *Canadian Geotechnical Journal*, 27(1): 151–158.
- Robertson, P.K. 2009a. Interpretation of cone penetration tests—a unified approach. *Canadian Geotechnical Journal*, 46: 1337–1355.
- Robertson, P.K. 2009b. Interpretation of cone penetration tests—a unified approach. *Journal of Geotechnical and Geoenvironmental Engineering*, ASCE. 135(11): 1762–1771.
- Robertson, P.K. 2010a. Evaluation of Flow Liquefaction and Liquefied strength Using the Cone Penetration Test. *Journal of Geotechnical and Geoenvironmental Engineering*, ASCE, 136(6): 842–853.
- Robertson, P.K. 2010b. Soil behaviour type from the CPT: an update. *2nd International Symposium on Cone Penetration Testing*, CPT’10, Huntington Beach, CA, USA. Paper No. 2–56. Available in CD-Rom or in: www.cpt10.com
- Robertson, P.K. 2010c. Estimating in-situ state parameter and friction angle in sandy soils from the CPT. *2nd International Symposium on Cone Penetration Testing*, Paper No. 2-43. CD-Rom or in: www.cpt10.com
- Robertson, P.K. 2012. In situ soil testing: from mechanics to interpretation”. 5th J.K. Mitchell Lecture, *Geotechnical & Geophysical Site Characterization*. Proc. ISC’4. Poto de Galinhas. Vol. 1. A. Balkema, CRS-Taylor & Francis.
- Robertson, P.K. & Campanella, R.G. 1986. Estimating Liquefaction Potential of Sands Using the Flat Plate Dilatometer. *Geotechnical Testing Journal*, ASTM. 9(1): 38–40.
- Robertson, P.K. & Wride, C.E. 1998. Evaluating cyclic liquefaction potential using the cone penetration test. *Canadian Geotechnical Journal*, 35: 442–459.
- Robertson, P.K., Woeller, D.J. & Finn, W.D.L. 1992. Seismic Cone Penetration Test for Evaluating Liquefaction Potential. *Canadian Geotechnical Journal*, 29(4): 686–695.
- Robertson, P.K., et al. 2000. The Canadian liquefaction experiment: An overview. *Canadian Geotechnical Journal*, 37: 499–504.
- Salem, H.S. 2000. Poisson’s ratio and the porosity of surface soils and shallow sediments, determined from seismic compressional and shear wave velocities. *Géotechnique*, 50(4): 461–463.
- Schmertmann, J.H., Baker, W., Gupta, R. & Kessler, K. 1986. CPT/DMT Quality Control of Ground Modification at a Power Plant”. *Proc. In Situ ’86, ASCE Spec. Conf. on “Use of In Situ Tests in Geot. Engrg.”*, Virginia Tech, Blacksburg, ASCE Geotech. Special Publ. No. 6, 985–1001.
- Schnaid, F. 2005. Geo-characterisation and properties of natural soils by in situ tests. Keynote *Lecture*. 16th ICSMGE, Osaka, Vol. 1, 3–45. Millpress, Rotterdam.
- Schnaid, F. 2009. *In Situ Testing in Geomechanics—The Main Tests*. Taylor & Francis, London, 327.
- Schnaid, F., Bedin, J. & Costa Filho, L.M. 2007. Piezocone in silty tailing materials. *Studia Geotechnical et Mechanica*, Polonia, Special Issue, No. 1-2, 151–162.
- Schnaid, F., Bedin, J. & Costa Filho, L.M. 2008. Drainage characterization of tailings from in situ. *Geotechnical & Geophysical Site Characterization*. Proc. ISC’3, Taiwan. CD-Rom. Taylor & Francis.
- Schnaid, F., Bedin, J., Vina da Fonseca, A. & Costa Filho, L. de M. al. 2012. Stiffness and strength governing tailings static liquefaction. *Journal of Geotechnical and Geoenvironmental Engineering*, ASCE. Accepted.
- Schnaid, F., Lehane, B.M. & Fahey, M. 2004. In Situ Test Characterization of Unusual Geomaterials. Keynote *Lecture*. *Geotechnical & Geophysical Site Characterization*. Proc. ISC’2—Porto. Vol. 1, 49–74. Millpress, Rotterdam.
- Schneider, J.A., McGillivray, A.V. & Mayne, P.W. 2004. Evaluation of SCPTU intra-correlations at sand sites in the lower Mississippi River Valley, USA. *Geotechnical & Geophysical Site Characterization*. Proc. ISC’2—Porto. Vol. 1, pp. 1003–101. Millpress, Rotterdam.
- Schneider, J.A. & Moss, R.E.S. 2011. Linking cyclic stress and cyclic strain based methods for assessment of cyclic liquefaction triggering in sands. *Géotechnique Letters*, Vol. 1 (doi: 10.1680/geolett.11.00021).
- Senneset, K., Sandven, R. & Janbu, N. 1989. Evaluation of soil parameters from piezocone tests. Transportation Research Record 1235, National Research Council, Washington, D.C., pp. 24–37.
- Sherif, M.A., Ishibashi, I. & Tsuchiya, C. 1977. Saturation effect on initial soil liquefaction. *J. Geotechnical Engineering Division*, ASCE, Vol. 103, 914–917.

- Skempton, A.W. 1954. The pore–pressure coefficients A and B. *Géotechnique*, 4(4): 143–147.
- Tai, P-H., Juang, D-H., Kung, G. T-C. & Juang, C.H. 2009. Simplified DMT-based methods for evaluating liquefaction resistance of soils. *Engineering Geology*, Vol. 103, 13–22. Elsevier (doi:10.1016/j.enggeo.2008.07.008).
- Tatsuoka, F., Jardine, R.J., Lo Presti, D., Di Benedetto, H. & Kodaka, T. 1997. Theme Lecture: *Characterising the pre-failure deformation properties of geomaterials*. 14th Int. Conf. SMFE, Hamburg, Vol. 4, 2129–216.
- Terzaghi, K. 1925. Structure and volume of voids of soils. Pages 10, 11, 12 and part of 13 of *Erdbaumechanik auf Bodenphysikalischer Grundlage*, translated by A. Casagrande in *From Theory to Practice in Soil Mechanics*, John Wiley & Sons, 146–148.
- Valle Molina. 2006. Measurements of V_p and V_s in dry, unsaturated and saturated sand specimens with piezoelectric transducers. PhD thesis Texas University at Austin, Texas.
- Verdugo, R. & Ishihara, K. 1996. The steady state of sandy soils. *Soils and Foundations*, 36(2): 81–91.
- Viana da Fonseca, A., Carvalho, J., Ferreira, C., Santos, J.A., Almeida, F., Pereira, E., Feliciano, J., Grade, J. & Oliveira, A. 2006. Characterization of a profile of residual soil from granite combining geological, geophysical and mechanical testing technique. *Geotech. and Geological Engineering*, 24(5): 1307–1348.
- Viana da Fonseca, A., Coop, M.T., Fahey, M. e Consoli, N. 2011. The interpretation of conventional and non-conventional laboratory tests for challenging geotechnical problems. (*Keynote Lecture*). *Deformation Characteristics of Geomaterials*, Vol. 1, pp. 84–119. IOS Press.
- Viana da Fonseca, A., Ferreira, C. & Fahey, M. 2009. A framework interpreting bender element tests, combining time-domain and frequency-domain methods. *Geotechnical Testing Journal*, ASTM. 32(2): 1–17.
- Vick, S.G. 1983. Planning, design and analysis of tailings dams. John Wiley & Sons Inc., New York.
- Vieira Faria, N., Viana da Fonseca, A. & Ferreira, C. 2006. Saturation process in triaxial tests. *Geotecnia*, Vol. 104, 31–42, SPG, Lisboa. (In Spanish).
- Wagener, F., Craig, H.J., Blight, G.E., McPhail, G., Williams, A.A.B. & Strydom, J.H. 1998. The Merriespruit tailings dam failure—a review. In Proceedings of the Conference.
- Wride, C.E., Robertson, P.K., Biggar, K.W., Campanella, R.G., Hofmann, B.A., Hughes, J.M.O., Küpper, A. & Woeller, D.J. 2000. In-Situ testing program at the CANLEX test sites. *Canadian Geotechnical Journal*, 37(3): 505–529.
- Wroth, C.P. & Bassett, R.H. 1965. A stress–strain relationship for the shearing behaviour of a sand. *Géotechnique*, 15(1): 32–56.
- Yamamuro J.A., Covert, K.M. & Lade, P.V. 1999. Static and cyclic liquefaction of silty sands. In Physics and mechanics of soil liquefaction. International Workshop, Lade, P.V. & Yamamuro, J.A., Eds, Baltimore, Maryland, USA. Balkema, 55–66.
- Yamamuro, J.A. & Lade, P.V. 1997. Static liquefaction of very loose sands. *Canadian Geotechnical Journal*, 34, No. 6, 905–917. Doi:10.1139/cgj-34-6-905.
- Yamamuro, J.A. & Lade, P.V. 1998. Steady-state concepts and static liquefaction of silty sands. *Journal of Geotechnical and Geoenvironmental engineering*, 124(9): 868–877.
- Yang, J. 2002. Non–uniqueness of flow liquefaction line for loose sand, *Géotechnique*, 52(10): 757–760.
- Yang, J. & Sato, T. 2001. Analytical study of saturation effects on seismic vertical amplification of a soil layer, *Géotechnique*. 51(2): 161–165.
- Yoshimi, Y., Tanaka, K. & Tokimatsu, K. 1989. Liquefaction resistance of a partially saturated sand. *Soils & Foundations*. 29: 157–162.
- Yu, H.S. 2004. In situ soil testing: from mechanics to interpretation”. 1st J.K. Mitchell Lecture, *Geotechnical & Geophysical Site Characterization*. Proc. ISC’2—Porto, Vol. 1, 3–38. Milpress, Netherlands.